JOURNAL OF Evolutionary Biology

doi: 10.1111/j.1420-9101.2012.02598.x

The effects of stochastic and episodic movement of the optimum on the evolution of the G-matrix and the response of the trait mean to selection

A. G. JONES*, R. BÜRGER†, S. J. ARNOLD‡, P. A. HOHENLOHE§ & J. C. UYEDA‡

*Department of Biology, Texas A&M University, College Station, TX, USA
†Institut für Mathematik, Universität Wien, Wien, Austria
‡Department of Zoology, Oregon State University, Corvallis, OR, USA
§Department of Biological Sciences and Institute for Bioinformatics and Evolutionary Studies, University of Idaho, Moscow, ID, USA

Keywords:

enhancement effect;
evolution in changing environments;
genetic drift;
heritability;
moving optimum;
pleiotropy;
selection gradient.

Abstract

Theoretical and empirical results demonstrate that the **G**-matrix, which summarizes additive genetic variances and covariances of quantitative traits, changes over time. Such evolution and fluctuation of the **G**-matrix could potentially have wide-ranging effects on phenotypic evolution. Nevertheless, no studies have yet addressed **G**-matrix stability and evolution when movement of an intermediate optimum includes large, episodic jumps or stochasticity. Here, we investigate such scenarios by using simulation-based models of **G**-matrix evolution. These analyses yield four important insights regarding the evolution and stability of the **G**-matrix. (i) Regardless of the model of peak movement, a moving optimum causes the **G**-matrix to orient towards the direction of net peak movement, so that genetic variance is enhanced in that direction (the variance enhancement effect). (ii) Peak movement skews the distribution of breeding values in the direction of movement, which impedes the response to selection. (iii) The stability of the **G**-matrix is affected by the overall magnitude and direction of peak movement, but modes and rates of peak movement have surprisingly small effects (the invariance principle). (iv) Both episodic and stochastic peak movement increase the probability that a population will fall below its carrying capacity and go extinct. We also present novel equations for the response of the trait mean to multivariate selection, which take into account the higher moments of the distribution of breeding values.

Introduction

The **G**-matrix of quantitative genetics plays a central role in theory for the evolution of phenotypic traits, especially those affected by many genes and environmental factors (Lande, 1979). The **G**-matrix provides a summary of additive genetic variances and covariances for a suite of phenotypic traits, so its importance stems from the central role of genetic variation in evolutionary processes. For example, the additive genetic variances recorded in the **G**-matrix provide an indication of the potential for trait means to be altered by evolutionary mechanisms such as natural selection or genetic drift (Arnold *et al.*, 2001; Steppan *et al.*, 2002). In addition, the genetic covariances summarized by the **G**-matrix provide a window into the extent to which evolutionary change in one trait is expected to affect the evolution of other measured traits, whose values may in part be determined by pleiotropic or linked loci (Lande, 1979; Arnold *et al.*, 2001). Despite its central role, the evolution and stability of the **G**-matrix remain outstanding, incompletely resolved problems (Jones *et al.*, 2003; Arnold *et al.*, 2008). The lack of complete resolution reflects the difficulty of finding analytical characterizations of **G** as a function of underlying processes, as well as the limitations of empirical studies in which **G**-matrices are sampled from natural or

Correspondence: Adam G. Jones, Department of Biology, Texas A&M University, 3258 TAMU, College Station, TX 77843, USA.
Tel.: 1 979 845 7774; fax: 1 979 845 2891;
e-mail: agjones@neo.tamu.edu

experimental populations and compared (Turelli, 1988; Steppan *et al.*, 2002; Arnold *et al.*, 2008). Because of these difficulties and limitations, simulation studies of the **G**-matrix have emerged as a powerful and complementary alternative to analytical theory and comparative studies (Jones *et al.*, 2003, 2004, 2007; Guillaume & Whitlock, 2007; Revell, 2007; Arnold *et al.*, 2008; Yeaman & Guillaume, 2009). Although largely restricted to the case of additive genetic effects (the simplest genotype-to-phenotype map), simulation studies yield many insights into the evolution and stability of the **G**-matrix.

A significant limitation of the simulation studies conducted so far is that they have not fully explored conditions that may contribute to **G**-matrix instability. For example, consider the case of traits evolving on an adaptive landscape with a single adaptive peak or optimum. Turelli (1988) argued that **G** would be especially unstable if the optimum were prone to episodes of large displacements. Although other cases of moving optima have been studied – steady movement (Jones *et al.*, 2004) or erratic movement about a fixed position (Revell, 2007) – the cases of episodic and stochastic movement have not been addressed, an unfortunate lapse because both might yield illuminating instances of instability. The neglect of the episodic case is particularly unfortunate because this model of peak movement appears to be more consistent with known evolutionary trends than any other proposed model (Estes & Arnold, 2007; Uyeda *et al.*, 2011).

The goals of this article are to explore the evolution and stability of the **G**-matrix when an intermediate optimum moves episodically or stochastically, with the justification that these cases might be both common in nature and especially conducive to instability of **G**. We compare these results with those for an optimum that moves at the same rate every generation, thereby identifying the influence of the mode of peak movement on various descriptors of the size, shape and stability of the **G**-matrix. We provide new theory that demonstrates and quantifies the role of skewness of breeding values induced by multivariate selection. To achieve greater power to detect systematic effects, we employ larger population sizes, stronger stabilizing selection and longer simulation runs than in our past study of a steadily moving optimum (Jones *et al.*, 2004). Finally, we evaluate the effect of **G**-matrix instability on data analyses that assume the **G**-matrix is constant. In particular, we determine how estimation of the net selection gradient (net-**β**; Lande, 1979) is affected by skewness of the breeding values and by the instability in **G** induced by different modes of peak movement.

Methods

The simulation model

Our model uses a Monte Carlo approach to simulate a diploid, sexually reproducing population with two phenotypic traits. The model, an extension of univariate models of the evolution of additive genetic variance (Bürger *et al.*, 1989; Bürger & Lande, 1994; Bürger & Lynch, 1995), has been described in detail elsewhere (Jones *et al.*, 2003, 2004). Each simulation run starts with a population of N diploid adults. The life cycle consists of (i) random, monogamous mating, (ii) production of progeny, including mutation and free recombination, (iii) viability selection and (iv) random culling of the population to a carrying capacity of N adults. The two quantitative traits are determined by n additive, pleiotropic loci. Hence, each allele at each locus potentially affects both traits, and allelic effects are summed across loci to determine an individual's breeding (additive genetic) value for each trait. To simulate environmental variance, we determine an individual's vector of phenotypic values by adding to each breeding value a random number drawn from a normal distribution with mean zero and variance of unity. The parameters and variables used in our model are summarized in Table 1.

During the progeny-production phase, we choose gametes at random to be affected by mutation. We assume a uniform per-locus mutation rate of μ. We draw a pseudorandom number between 0 and 1 from a uniform distribution and assume that a gamete carries a new mutation if the random number is less than $n\mu$. For gametes affected by a mutation, we choose a locus at random and change the allelic effects at that locus in the gamete under consideration in accord with the continuum of allele models (Crow & Kimura, 1964). Because every locus is pleiotropic, each allele has two allelic effects, one for each of the two phenotypic traits. Thus, we simulate mutational effects by drawing two numbers from a bivariate normal distribution with means of zero, variances of α_1^2 and α_2^2 and a correlation of r_μ. These mutational effects are then added to the existing allelic effects at the locus. Note that α_1^2, α_2^2 and r_μ (i.e. the mutational variances for the two traits and the mutational correlation) together describe the mutational matrix (**M**) for a locus. In this model, we make the simplifying assumption that all loci have identical mutational matrices and that the mutational matrix remains constant throughout a particular run (i.e. **M** is a parameter of the model).

We impose selection by assuming a single-peaked individual selection surface with the shape of a Gaussian distribution. Hence, the fitness, $W(\mathbf{z})$, of an individual with phenotype $\mathbf{z}$ (a column vector of phenotypic values) depends on its phenotypic distance from the bivariate optimum, according to the equation:

$$W(\mathbf{z}) = \exp\left[-\frac{1}{2}(\mathbf{z}-\boldsymbol{\theta})^{\mathrm{T}}\boldsymbol{\omega}^{-1}(\mathbf{z}-\boldsymbol{\theta})\right], \qquad (1)$$

where $\boldsymbol{\theta}$ is a column vector of trait optima, T represents matrix transposition and the matrix $\boldsymbol{\omega}$ describes the orientation and curvature of the individual selection surface (Lande, 1979). For the two-trait case, $\boldsymbol{\omega}$ is a 2×2

Table 1 Variables and parameters used in the model

Variable	Description
N	Number of diploid adults in the sexually reproducing population (1024 in the present study)
n	Number of pleiotropic loci (set to 50 in this analysis)
μ	Mutation rate per locus per meiosis (held at 0.0002 for this study)
α_1^2, α_2^2	Mutational variances for trait 1 and trait 2 (the diagonal elements of the mutational matrix, **M**)
r_μ	Mutational correlation (the standardized off-diagonal element of the **M**-matrix)
$\mathbf{z}$	A two-element column vector of trait values (z_1 and z_2 are the values for trait 1 and trait 2)
$\boldsymbol{\theta}$	A two-element column vector of trait optima (θ_1 and θ_2 are the optima for the traits)
$W(\mathbf{z})$	The fitness of an individual with phenotype **z**
ω_{11}, ω_{22}	The width of the selection surface for traits 1 and 2 (the diagonal elements of $\boldsymbol{\omega}$)
$r_{\boldsymbol{\omega}}$	The selectional correlation (the standardized off-diagonal element of $\boldsymbol{\omega}$)
B	The number of offspring per reproducing adult (set to 2 in the present analysis)
$\Delta\boldsymbol{\theta}$	A two-element column vector describing the per-generation change in the position of the optimum
$\sigma_{\theta 1}^2, \sigma_{\theta 2}^2$	The amount of stochasticity in the position of the optimum for traits 1 and 2, respectively
G_{11}, G_{22}, G_{12}	The elements of the **G**-matrix: the additive genetic variances and the additive genetic covariance
r_g	The additive genetic correlation (i.e. $G_{12}/\sqrt{G_{11}G_{22}}$)
λ_1, λ_2	The eigenvalues of the **G**-matrix
ϕ	The angle of the leading eigenvector of **G** on a graph with trait 1 on the x-axis and trait 2 on the y-axis
Σ	The size of the **G**-matrix, defined as $G_{11} + G_{22}$ or equivalently $\lambda_1 + \lambda_2$
ε	The eccentricity of **G**, defined as the smaller eigenvalue divided by the larger eigenvalue
Δ	When preceding the above variables, indicates the per-generation change in the variable of interest
$\boldsymbol{\beta}$	A two-element column vector of directional selection gradients (β_1 and β_2) on the two traits (eqn 2)
$\boldsymbol{\beta}_T$	Net-$\boldsymbol{\beta}$, which is the sum of the per-generation $\boldsymbol{\beta}$ values over the time period of interest
$\mathbf{x}$	A two-element vector of breeding values (i.e. additive genetic values) for the two traits of an individual
P	The phenotypic covariance matrix, with elements P_{11}, P_{22} and P_{12}.
E	The environmental covariance matrix, so **P** = **G** + **E**, and in our model **E** has diagonal values of 1 and zeros elsewhere
L	A two-element column vector of the lag, either observed ($\boldsymbol{\theta} - \mathbf{z}$) or expected (indicated by subscripts) under a Gaussian model (eqn 3)
$\boldsymbol{\Lambda}$	A two-element column vector of the expected lag, taking the skewness in breeding values into account (eqn 4)
$\boldsymbol{\Omega}$	A matrix describing the curvature of the fitness surface for breeding values ($\boldsymbol{\Omega} = \boldsymbol{\omega} + \mathbf{E}$)
$\nabla_{\mathbf{x}}\overline{W}$	The first-order selection gradient with respect to breeding values (i.e. $\boldsymbol{\beta}$)
$\nabla_{\mathbf{G}}\overline{W}$	The second-order selection gradient with respect to the genetic covariances (necessary for theory of the lag including skewness)
$\boldsymbol{\tau}$	A two-element vector of the Turelli effect for each trait, which arises due to covariance between **G** and $\boldsymbol{\beta}$ (eqn 9)

matrix, with diagonal elements ω_{11} and ω_{22}, which describe the width (and also curvature) of the individual selection surface. Smaller values of these diagonal elements indicate stronger stabilizing selection. Both off-diagonal elements are given by ω_{12}, which determines the strength of correlational selection. In the model, $W(\mathbf{z})$ is the probability that an individual survives from birth to adulthood, with a maximum value of one for individuals at the optimum. We represent the strength of correlational selection as a standardized coefficient, analogous to a correlation coefficient, $r_\omega = \omega_{12} \ /\sqrt{\omega_{11}\omega_{22}}$. In our runs, we set stabilizing selection at a moderately strong value, $\omega_{11} = \omega_{22} = 9$, and vary $r_{\boldsymbol{\omega}}$ from -0.9 to 0.9.

From the survivors of selection, we choose N individuals at random to represent the adults of the current generation, which then mate at random to produce the next generation of progeny. To ensure that results are comparable across simulation runs, we terminate a run if fewer than N individuals survive selection and calculate summary statistics only for parameter combinations under which all replicate populations survive for the entire duration of the simulation. We record the parameter combinations under which some runs fall below the carrying capacity, because this drop in population size is a necessary precursor to population extinction. In models with a moving optimum, a drop below the carrying capacity will almost always result in rapid population extinction, because the loss of genetic variation associated with the reduction in effective population size exacerbates the problem that the population cannot evolve quickly enough to keep up with the moving optimum. We assume an equal sex ratio among the N adults and impose a monogamous mating system. Each breeding pair produces exactly $2B$ offspring (i.e. B is the number of offspring per reproducing adult), resulting in effective population sizes larger than the census population sizes (Bürger & Lande, 1994; Jones *et al.*, 2003). Because the effects of population size on **G**-matrix stability are well understood, we focus on a population of 1024 adults, which corresponds to an effective population size of 1366 (Jones *et al.*, 2003, 2004).

Each run of the simulation starts with a genetically monomorphic population, and we allow genetic variation to accumulate during an initial 10 000

generations of evolution under a stationary optimum. We follow these generations with 2000 generations of directional selection under the model of peak movement of interest, allowing the population to equilibrate with respect to the moving optimum. Finally, the simulations run for an additional 4000 experimental generations, during which the optimum continues to move according to the model of interest and we tally genetic variables every generation. We typically replicate each combination of parameters in 20 independent simulation runs and calculate averages within and between these runs (Jones *et al.*, 2003, 2004).

Rates and modes of peak movement

We employ three models of peak movement (Fig. 1) and perform control simulations under a stationary optimum. In the first model of peak movement, steady directional movement, the bivariate optimum shifts every generation by a small amount, k. In the second model of peak movement, the optimum moves at the same overall rate as in the steady directional movement model, except that the bivariate optimum moves instantaneously a correspondingly large distance every 100 or 250 generations and otherwise is stationary. In this model, the optimum spends long periods of time in a stationary position, but this stasis is punctuated by large jumps. For our third type of peak movement, we use a stochastic model (deterministic change with Brownian motion) in which the position of the optimum for a trait at generation t (i.e. θ_t) is a function of the old position ($\theta_{t\text{-}1}$), a constant amount of change (k) and a component of random change (ε_θ), so that the change in optimum at generation t is

$$\Delta\theta_t = \theta_t - \theta_{t-1} = k + \varepsilon_\theta$$

where ε_θ is normally distributed with mean 0 and variance σ^2_θ.

We choose modes and rates of peak movement that bracket empirical observations. Stasis is the predominant pattern of evolution observed in a large sample of neontological and palaeontological studies, but substantial evolutionary change is also observed in a significant subset of cases (Gingerich, 2001; Estes & Arnold, 2007; Uyeda *et al.*, 2011). At the two rates of evolutionary change we employ (0.006 or 0.008 phenotypic standard deviations per generation), the optimum moves 23–33 phenotypic standard deviations in 4000 generations. At this timescale, no observations in Gingerich's (2001) extensive data set show as much evolutionary change. On the other hand, Kinnison & Hendry (2001) find a median rate of 0.006 in a large sample of studies on shorter timescales (< 300 generations), a value that closely matches those used in our simulations. Thus, we use rates of peak movement that approximate those

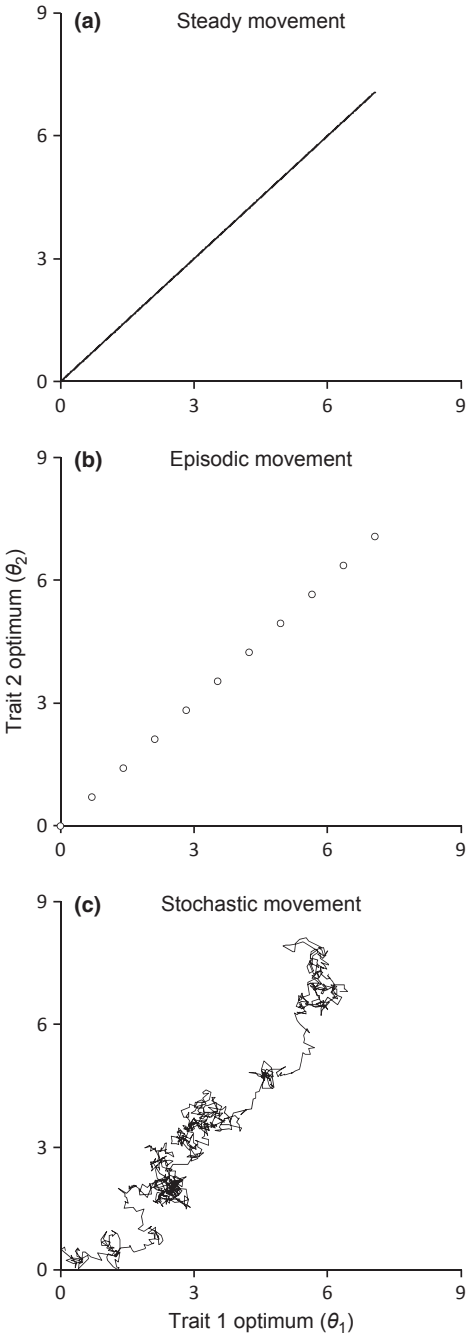

Fig. 1 Schematic portrayals of the three modes of peak movement used in the simulations. In all of these figures, the peak starts at (or near) the origin and moves up and to the right. In (a), the peak moves every generation in a constant direction at a constant rate. In (b) and (c), the average rate and direction are as in (a). In (b), the peak remains stationary for many generations and then jumps to the new position. In the case shown, the jumps occur every 100 generations. In (c), the peak moves every generation, but peak movement also includes an element of stochasticity each generation. In this case, the stochasticity variance parameter (σ^2_θ) is 0.01.

observed over relatively short-term periods of evolution but that would be unlikely to persist over extremely long periods of time.

For each model of peak movement (Fig. 1), we investigate three different directions of movement of the optimum phenotype. In the first case, the optima of both traits increase, so the bivariate optimum moves up and to the right on a plot with trait one values on the *x*-axis and trait two values on the *y*-axis. In this first case we represent the movement by ↗. In the second case, the optimum for trait one increases, whereas the optimum of trait two remains stationary on average (→). In the final case, the optimum for trait one increases and the optimum for trait two decreases (↘). As noted above, we also investigate a stationary optimum (●) for comparison.

Characterization of the G-matrix

We quantify the **G**-matrix in three different ways, following the precedent set by Jones *et al.* (2003, 2004). The simplest characterization is to consider the individual elements of the two-trait **G**-matrix: the trait one additive genetic variance (G_{11}), the trait two additive genetic variance (G_{22}) and the additive genetic covariance between the two traits (G_{12}). The genetic correlation (r_g) also provides a useful way of comparing genetic constraints across **G**-matrices. The second approach that we use to quantify the **G**-matrix involves examining the eigenvectors and eigenvalues of the matrix. This approach is useful, because the leading eigenvector of the **G**-matrix indicates the direction in phenotypic space with the maximum amount of additive genetic variance (i.e. the genetic line of least resistance; Schluter, 1996). We quantify the eigenvector as an angle in degrees relative to the *x*-axis on a plot with the *x*-axis representing trait one and the *y*-axis representing trait two. Thus, we can fully describe the **G**-matrix by using the angle of the leading eigenvector (ϕ) and the eigenvalues (λ_1 and λ_2). A third way to characterize the **G**-matrix is to use the size Σ, which is equal to the sum of the eigenvalues (or $G_{11} + G_{22}$), as a measure for the total amount of variation; the inverse measure ε of eccentricity, which we define as the smaller eigenvalue divided by the larger eigenvalue; and the angle ϕ. We use two sets of measures of stability of the **G**-matrix. One describes the rate at which the **G**-matrix changes per generation, represented by the mean absolute values of the per-generation changes in each of these variables and denoted by a Δ preceding the symbol for the relevant variable. We also report the standard deviations of **G**-matrix descriptors across all generations within a simulation run as measures of the extent to which variables experience excursions from their long-term (i.e. within-run) averages.

Theoretical background

The evolution of the **G**-matrix on a landscape with a moving optimum is closely tied to theory for the response of the multivariate phenotypic mean to selection and the lag of that mean relative to the optimum, so we present here some critical equations that will be necessary to interpret our results. One feature of our model, or any theoretical or empirical example of evolution in response to a moving optimum, is that the population mean will lag behind the optimum. In the present study, we use the difference between the mean phenotype and the optimum as a measure of the strength of selection in any given generation (Lande, 1979). Assuming a Gaussian selection surface (eqn 1), the selection gradient $\boldsymbol{\beta}_t$ at time *t*, defined by $\nabla_{\bar{\mathbf{z}}}\overline{W}$ (see Appendix I), becomes the following column vector:

$$\boldsymbol{\beta}_t = (\boldsymbol{\omega} + \mathbf{P}_t)^{-1}(\boldsymbol{\theta}_t - \bar{\mathbf{z}}_t), \tag{2}$$

where $\mathbf{P}_t$ is the phenotypic variance–covariance matrix at time *t*, $\boldsymbol{\omega} + \mathbf{P}_t$ is the curvature of the adaptive landscape at time *t*, $\boldsymbol{\theta}_t$ is a column vector of trait optima at time *t*, and $\bar{\mathbf{z}}_t$ is a column vector of trait means at time *t*. We apply this equation every generation of a simulation run to calculate the true value of the net directional selection gradient, net-$\boldsymbol{\beta}$, that is, of $\boldsymbol{\beta}_T = \sum_{t=0}^{T-1} \boldsymbol{\beta}_t$ for that particular run (of length *T*).

If the optimum moves every generation at a constant rate, then, assuming the population does not go extinct, the phenotypic mean will equilibrate some distance behind the optimum, depending on the amount of additive genetic variance in the population, the shape of the selection surface and the rate at which the optimum moves. Under the assumption of a Gaussian distribution of breeding values (Lande, 1979), the expected lag is (Lynch & Lande, 1993; Jones *et al.*, 2004)

$$\mathbf{L} = \boldsymbol{\theta}_t - \bar{\mathbf{z}}_t = (\boldsymbol{\omega} + \mathbf{P})\mathbf{G}^{-1}\Delta\boldsymbol{\theta}, \tag{3}$$

where $\Delta\boldsymbol{\theta}$ is a vector of per-generation changes in the trait optima, and **P** is the phenotypic covariance matrix. Note that $\mathbf{P} = \mathbf{G} + \mathbf{E}$, where **E** is the environmental covariance matrix.

As we will see below, we find that in the case of a rapidly moving optimum and relatively strong curvature of the individual selection surface, eqn (3) consistently underestimates the amount of lag. Because such deviations can be caused by selection-induced skew in the distribution of breeding values, we derive equations for the response to selection and the multivariate lag, which take into account the third and higher moments of the distribution of breeding values. This theory is derived in Appendix I. In this paper, we focus primarily on the lag rather than the response of the mean to selection. However, it is important to keep in mind that the lag and the response to selection are intimately

related, because the population mean will equilibrate at a distance behind the optimum at which selection is sufficiently strong to produce a response that is equal to the rate at which the optimum is moving. Accounting for the skewness of the breeding distribution, our equation for the expected lag becomes

$$\Lambda \approx \Omega \mathbf{G}^{-1}\left(\Delta\boldsymbol{\theta} - \mathbf{C}\nabla_{\mathbf{G}}\overline{W}\right). \tag{4}$$

Here, $\boldsymbol{\Lambda}$ is a column vector whose elements represent the lag for each trait, $\boldsymbol{\Omega} = \boldsymbol{\omega} + \mathbf{E}$, $\nabla_{\mathbf{G}}\overline{W}$ is the 4-dimensional ('quadratic') selection gradient with respect to the genetic covariances (eqn A.9 in Appendix I), and $\mathbf{C}$ is the 2×4 matrix defined in Appendix I containing all third-order cumulants $c_{i,j}$ given by

$$c_{i,j} = \int (x_1 - \bar{x}_1)^i (x_2 - \bar{x}_2)^j p(\mathbf{x}) \mathrm{d}x,$$

where $p(\mathbf{x})$ denotes the distribution of breeding values, $\mathbf{x} = (x_1, x_2)$, and $i \geq 0$, $j \geq 0$, $i + j = 3$ (see eqn A.16 in Appendix I).

Equation (4) is straightforwardly derived from the following equation for the change of the vector $\bar{\mathbf{x}}(= \bar{\mathbf{z}})$ of mean additive genetic values,

$$\Delta\bar{\mathbf{x}} \approx \mathbf{G}\nabla_{\bar{\mathbf{x}}}\overline{W} + \mathbf{C}\nabla_{\mathbf{G}}\overline{W}, \tag{5}$$

where $\nabla_{\bar{\mathbf{x}}}\overline{W}$ is the directional selection gradient, because for our model we find that $\nabla_{\bar{\mathbf{x}}}\overline{W} = \boldsymbol{\Omega}^{-1}\Lambda$ and $\nabla_{\mathbf{G}}\overline{W} = -(1/2)\boldsymbol{\Omega}^{-1}$ (Appendix I). Equation (5) can be generalized to accommodate arbitrary fitness functions. Then, however, higher-order cumulants affect the response of the mean (eqn A.4 in Appendix I). The corresponding univariate theory was developed by Turelli & Barton (1990, 1994) and Bürger (1991); see Bürger (2000) for a comprehensive, unified treatment.

Equation (4) shows that a positively skewed distribution will increase the expected lag because with our fitness function $\nabla_{\mathbf{G}}\overline{W} = -(1/2)\boldsymbol{\Omega}^{-1}$. This result can be understood intuitively because with positive skew, the mode of the distribution will be left of the mean. Thus, a larger fraction of the population is under strong selection than with a symmetric distribution, but individuals near the mode harbour less genetic variance than would be expected under a Gaussian distribution. Consequently, for a given value of the additive genetic variance, a skewed distribution produces a smaller response to selection compared with a Gaussian distribution.

If we denote the entries of the 2×2 matrix $\boldsymbol{\Omega}^{-1}$ by a_{11}, a_{12}, and a_{22}, we obtain from eqn (4) the following representation for the lag in the two-trait case studied here:

$$\begin{pmatrix}\Lambda_1\\ \Lambda_2\end{pmatrix} = \tfrac{1}{2\det\mathbf{G}}\begin{pmatrix}(\omega_{11}+1)G_{22} - \omega_{12}G_{12} & \omega_{12}G_{11} - (\omega_{11}+1)G_{12}\\ \omega_{12}G_{22} - (\omega_{22}+1)G_{12} & (\omega_{22}+1)G_{11} - \omega_{12}G_{12}\end{pmatrix}\begin{pmatrix}2\Delta\theta_1 + a_{11}c_{3,0} + 2a_{12}c_{2,1} + a_{22}c_{1,2}\\ 2\Delta\theta_2 + a_{11}c_{2,1} + 2a_{12}c_{1,2} + a_{22}c_{0,3}\end{pmatrix}. \tag{6}$$

Finally, our analyses will require some theory related to the calculation of net-$\boldsymbol{\beta}$ and the Turelli effect (Jones *et al.*, 2004). Turelli (1988) pointed out that covariance between $\mathbf{G}$ and $\boldsymbol{\beta}$ could present problems for the reconstruction of net-$\boldsymbol{\beta}$, and he also predicted that such covariance would be most pronounced when selection is especially strong, such as immediately after a major shift in the optimum. This seemingly reasonable assertion is the motivation for our interest in the Turelli effect under an episodic model of peak movement. If we have knowledge of the average $\mathbf{G}$-matrix, $\bar{\mathbf{G}}$, over some time interval of interest, and we know how much the multivariate phenotypic mean has changed over that interval ($\Delta\bar{\mathbf{z}}_T$), then we can calculate the total selection that has operated on the phenotypic mean over the time interval as the net directional selection gradient $\boldsymbol{\beta}_T$ (Lande, 1979). If the $\mathbf{G}$-matrix is constant over evolutionary time, then the contemporary $\mathbf{G}$-matrix is equal to the average $\mathbf{G}$-matrix over the timescale of interest, a convenience that greatly facilitates the application of this theory because then

$$\boldsymbol{\beta}_T = \sum_{t=0}^{T-1}\boldsymbol{\beta}_t = \sum_{t=0}^{T-1}\bar{\mathbf{G}}^{-1}\Delta\bar{\mathbf{z}}_t = \mathbf{G}^{-1}\Delta\bar{\mathbf{z}}_T. \tag{7}$$

However, Turelli (1988) pointed out that even if the average $\mathbf{G}$-matrix is known, the reconstruction of net-$\boldsymbol{\beta}$ can be derailed if $\boldsymbol{\beta}$ and $\mathbf{G}$ covary. Because $\Delta\bar{\mathbf{z}}_T = \sum_{t=0}^{T-1}\mathbf{G}_t\boldsymbol{\beta}_t$, we find

$$\begin{aligned}\boldsymbol{\beta}_T &= \bar{\mathbf{G}}^{-1}\Delta\mathbf{z}_T - \bar{\mathbf{G}}^{-1}\sum_{t=0}^{T-1}\mathbf{G}_t\boldsymbol{\beta}_t + \bar{\mathbf{G}}^{-1}\bar{\mathbf{G}}\sum_{t=0}^{T-1}\boldsymbol{\beta}_t\\ &= \bar{\mathbf{G}}^{-1}\Delta\mathbf{z}_T - \bar{\mathbf{G}}^{-1}\sum_{t=0}^{T-1}(\mathbf{G}_t - \bar{\mathbf{G}})\boldsymbol{\beta}_t.\end{aligned} \tag{8}$$

If we define the Turelli effect (Jones *et al.*, 2004) as

$$\boldsymbol{\tau} = \bar{\mathbf{G}}^{-1}\sum_{t=0}^{T-1}(\mathbf{G}_t - \bar{\mathbf{G}})\boldsymbol{\beta}_t, \tag{9}$$

then we can rewrite eqn (8) as

$$\boldsymbol{\beta}_T = \bar{\mathbf{G}}^{-1}\Delta\mathbf{z}_T - \boldsymbol{\tau}. \tag{10}$$

Thus, in the two-trait case, the Turelli effect will be quantified by a column vector with two elements, τ_1 and τ_2, which indicate the extent to which covariance between $\boldsymbol{\beta}$ and $\mathbf{G}$ presents a problem for the reconstruction of net-$\boldsymbol{\beta}$.

Results

The effects of episodic and stochastic peak movement on the magnitude and shape of G

The mode of peak movement can affect both the configuration and the stability of the **G**-matrix. In Table 2, we compare the results of a stationary optimum, a steadily moving optimum, episodic peak movement and stochastic peak movement for a subset of parameter combinations. For the sake of clarity, we present representative results only. In actuality, we investigated selectional correlations of −0.9, −0.85, −0.75, −0.5, −0.25, 0, 0.25, 0.5, 0.75, 0.85 and 0.9 and mutational correlations of 0, 0.25, 0.5, 0.75 and 0.9 in all pairwise combinations of mutational and selectional correlations. Furthermore, we studied all of these combinations of mutational and selectional correlations in combination with each model of peak movement, with several different values for the interval between peak shifts and the magnitude of stochasticity in movement of the optimum. The results shown in Table 2 represent general patterns, which occurred across the wide array of parameters we investigated.

One extremely robust result, shown here and in other studies, is that, relative to a stationary optimum, peak movement always increases the size of the **G**-matrix (G_{11}, G_{22}, λ_1, λ_2 and Σ) on average for populations that remain above their carrying capacity for the duration of the 4000 experimental generations. In almost all cases, this 'variance enhancement effect' increases **G**-matrix size by a substantial amount, ranging from increases of about 50% up to a factor of almost three. The degree of enhancement of additive genetic variance due to movement of the optimum depends upon the model of peak movement. Interestingly, episodic movement provides virtually the same increase in genetic variance as a steadily moving optimum (Table 2), even when the optimum jumps only every 250 generations by an amount 250 times greater than the single-generation peak shifts used in the steadily moving optimum model (resulting in the same amount of net change in the optimum over the 4000 generations of the simulation). Stochastic movement of the optimum, however, provides a greater enhancement of the genetic variance compared with deterministic movement (Table 2).

Table 2 The effects of different models of peak movement on aspects of the **G**-matrix and its stability. The first three columns show parameters describing the model of peak movement, with $\Delta\boldsymbol{\theta}$ showing the direction of peak movement (• means stationary; ↗ means $\Delta\theta_1 = \Delta\theta_2 = 0.0071$ on average per generation, → means $\Delta\theta_1 = 0.01$ and $\Delta\theta_2 = 0$; ↘ means $\Delta\theta_1 = 0.0071$ and $\Delta\theta_2 = -0.0071$). The second column indicates the interval between shifts of the optimum, and the third column indicates the amount of stochasticity in peak movement. The aspects of the **G**-matrix shown here include the additive genetic variances for traits one and two (G_{11} and G_{22}), the genetic correlation (r_g), the size of the **G**-matrix ($\Sigma = G_{11} + G_{22}$), the eccentricity (ε, which is the smaller eigenvalue of **G** divided by the larger eigenvalue) and the angle of the leading eigenvector of **G** (ϕ). We also show the average lag for the two traits, which is the optimum minus the phenotypic mean. Each of these values is a mean, calculated by averaging first across the 4000 generations of each run and then across 20 independent replicate runs under each combination of parameters. The last six columns show the average absolute change per generation in each aspect of the **G**-matrix. The values for ΔG_{11}, ΔG_{22}, $\Delta\Sigma$ and $\Delta\varepsilon$ are standardized by dividing by the mean, while Δr_g and $\Delta\phi$ are raw values. The following parameters are fixed: number of loci: $n = 50$; population size: $N = 1024$; per-locus mutation rate: $\mu = 0.0002$ per generation; mutational variances: $\alpha_1^2 = \alpha_2^2 = 0.05$; curvature of the selection surface: $\omega_{11} = \omega_{22} = 9$; selectional correlation: $r_\omega = 0$; mutational correlation: $r_\mu = 0.50$. For most variables, the standard errors are much smaller than the means, and the bottom row shows the mean standard error across the 20 independent simulation runs for each column. Also see Table S4 for average within-run standard deviations.

$\Delta\boldsymbol{\theta}$	Interval	$\sigma^2_{\theta 1} = \sigma^2_{\theta 2}$	G_{11}	G_{22}	r_g	Σ	ε	ϕ	L_1	L_2	ΔG_{11}	ΔG_{22}	Δr_g	$\Delta\Sigma$	$\Delta\varepsilon$	$\Delta\phi$
•	0	0	0.22	0.22	0.27	0.44	0.56	45.4	0.00	0.00	0.037	0.037	0.024	0.028	0.051	2.9
↗	1	0	0.50	0.49	0.44	0.99	0.39	44.7	0.14	0.14	0.036	0.036	0.020	0.028	0.051	1.5
↗	100	0	0.50	0.50	0.44	1.00	0.39	44.9	0.14	0.14	0.036	0.036	0.020	0.028	0.051	1.5
↗	250	0	0.50	0.50	0.46	0.99	0.37	45.1	0.14	0.14	0.036	0.036	0.020	0.028	0.051	1.4
↗	1	0.01	0.55	0.54	0.38	1.08	0.44	44.4	0.14	0.13	0.036	0.036	0.022	0.028	0.051	1.9
↗	1	0.02	0.58	0.55	0.35	1.13	0.47	41.7	0.13	0.11	0.036	0.036	0.022	0.028	0.051	2.2
→	1	0	0.56	0.37	0.23	0.93	0.52	23.4	0.25	−0.05	0.036	0.036	0.024	0.027	0.051	2.5
→	100	0	0.56	0.36	0.24	0.92	0.52	24.1	0.25	−0.05	0.036	0.036	0.024	0.027	0.051	2.4
→	250	0	0.57	0.37	0.24	0.94	0.51	23.8	0.24	−0.05	0.036	0.036	0.024	0.027	0.051	2.3
→	1	0.01	0.57	0.44	0.27	1.01	0.52	32.0	0.23	−0.05	0.036	0.036	0.023	0.027	0.051	2.6
→	1	0.02	0.58	0.50	0.26	1.08	0.55	35.9	0.22	−0.06	0.036	0.036	0.023	0.027	0.051	3.0
↘	1	0	0.44	0.44	0.06	0.88	0.75	16.9	0.21	−0.21	0.036	0.036	0.025	0.026	0.050	7.5
↘	100	0	0.45	0.44	0.07	0.89	0.76	18.5	0.21	−0.21	0.036	0.036	0.025	0.026	0.049	8.2
↘	250	0	0.43	0.44	0.06	0.87	0.76	19.4	0.21	−0.21	0.036	0.036	0.025	0.026	0.049	7.8
↘	1	0.01	0.48	0.48	0.15	0.95	0.67	36.5	0.20	−0.19	0.036	0.036	0.024	0.026	0.050	5.2
↘	1	0.02	0.53	0.53	0.19	1.06	0.63	40.7	0.18	−0.19	0.036	0.036	0.024	0.027	0.050	4.3
Mean SE of estimates			0.007	0.007	0.009	0.010	0.009	1.5	0.005	0.006	0.0005	0.0006	0.0001	0.0003	0.001	0.2

A few other differences between our models of peak movement are apparent from Table 2. The results in Table 2 assume a mutational correlation (r_μ) of 0.5, so that even when the optimum is stationary the population evolves a positive genetic correlation (r_g) between the two traits. When the optimum moves in a positive direction for both traits (↗), this movement along the genetic line of least resistance increases the value of r_g. However, the increase in genetic correlation is less pronounced when we introduce stochasticity into the movement of the optimum. This result occurs because, even though the net direction of movement of the optimum is along the genetic line of least resistance, the optimum sometimes moves in a direction that cuts across this line, creating a situation less favourable for the evolution of a strong genetic correlation. A similar effect is seen for the eccentricity (recall that smaller values indicate a more eccentric **G**-matrix; Table 2). A complementary effect occurs when the optimum moves in a positive direction for trait one but in a negative direction for trait two (↘). In this case, the optimum moves in a direction that is misaligned with the mutational matrix, a situation that disfavours the evolution of a strong genetic correlation relative to the case of a stationary optimum. However, the effect is less pronounced when the movement of the optimum includes stochasticity, because in these cases the optimum sometimes moves in a direction favourable for the evolution of a strong genetic correlation. Thus, stochasticity tends to temper the effects attributable to the direction of peak movement. Tables S1–S3 provide a more extensive comparison of the **G**-matrices and their per-generation changes under a wider variety of parameter combinations and lend additional support to the above summary of findings.

The conclusion that stochastic movement of the optimum dampens the effects of peak movement on **G**-matrix stability is especially obvious if we consider the stability of the angle, ϕ. The stability of the angle is a meaningful measure for the stability of **G**-matrix orientation only if there is sufficient eccentricity, for instance, if ε is less than about 0.8. Figure 2 shows the average per-generation changes in the angle of the **G**-matrix under a wide variety of values for the selectional and mutational correlations. One obvious feature of this figure is that the average dynamics of the change in the angle of **G** are nearly the same for steady movement as for episodic movement, provided the net change in the optimum is the same in both cases. In particular, cases of three-way alignment, for example, when both the mutational correlation and the selectional correlation are positive and the optimum moves up and to the right, are most favourable for stability of the angle. The least stable cases occur when the mutational correlation, selectional correlation and direction of optimum movement are not aligned (i.e. top row of graphs with negative selectional correlations or bottom row of graphs with positive selectional correlations). Figure 2 also shows an important difference between runs that include an element of stochasticity in the position of the optimum and those that do not in that stochasticity lessens the impact of the stabilizing and destabilizing effects of the direction of peak movement.

Assessing the effects of the model of peak movement on the stability of the G-matrix using variation in G-matrix characteristics

The average values of the variables describing the **G**-matrix are nearly identical between runs with steady movement and those with episodic movement (Table 2, Tables S1 and S2). In addition, the average values of these variables differ in some ways under a stochastically moving optimum, but are more similar than we might have expected *a priori* (Tables 2 and S3). However, even though the average values of these variables are similar, the dynamics of **G**-matrix evolution could be quite different under different models of peak movement if the genetic variances or covariances are more variable over time under certain models of movement of the optimum. Table S4 presents the within-run standard deviations of the **G**-matrix variables and shows that episodic peak movement has subtle effects on the extent to which aspects of the **G**-matrix and its between-generation change deviate from the mean over time. Given the conspicuous differences in the generation-to-generation dynamics of **G** under steady versus episodic peak movement (compare Figs 3 and 4), these tiny effects are unexpected. The lag, of course, is much more variable with episodic movement of the optimum, because the phenotypic mean is quite far from the optimum immediately after an episode of peak movement. A second observation from Table S4 is that, relative to steady movement, stochastic movement of the optimum has much larger effects on the stability of the **G**-matrix than episodic movement; in general, stochastic movement leads to increased standard deviations.

For example, the variability in the lag is much higher in the stochastic model relative to the episodic and steady models, even though the mean lag is actually smaller in the stochastic model of peak movement. This higher variability in the lag is due to the optimum moving unpredictably, such that the population mean can be displaced in any direction relative to the optimum in any given generation.

Patterns of G-matrix evolution under episodic and stochastic peak movement

Some of the differences between the various models of peak movement are apparent from inspection of the values of variables during sample simulation runs. Figure 3 shows a time series of the size of the **G**-matrix, the eccentricity, the angle of **G** and the

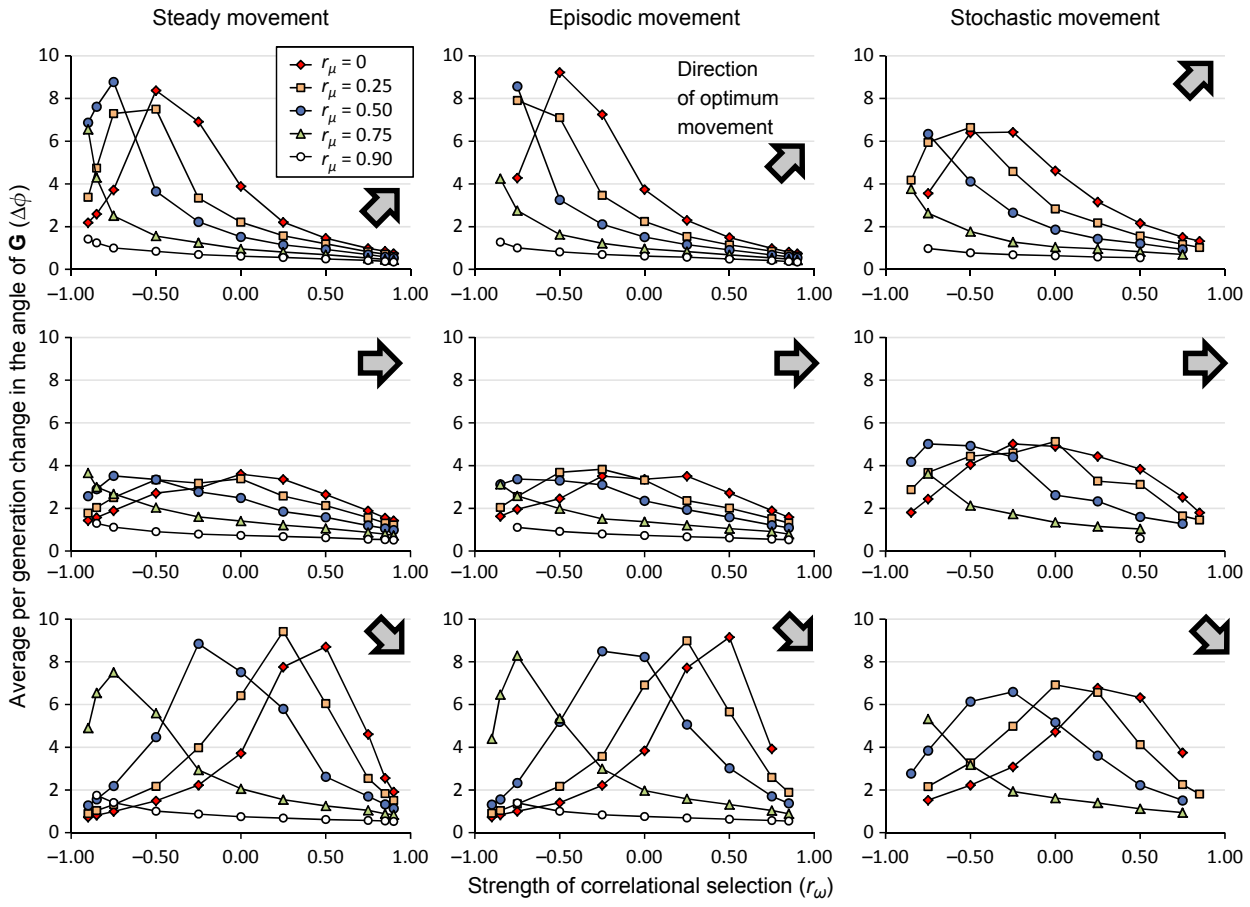

Fig. 2 The average per-generation change in the angle, $\Delta\phi$, of **G** as a function of the strengths of correlational selection and mutational correlation. The left column shows results under steady movement, in which the optimum moves every generation by a small amount. The middle column shows results for an episodically moving optimum that jumps every 100 generations, but moves at the same long-term average rate as in the steady movement case. The right column shows the case in which the optimum moves every generation, but with stochasticity ($\sigma^2_{\theta 1} = \sigma^2_{\theta 2} = 0.01$). Mutational correlations ranged from 0 to 0.9, and selectional correlations ranged from −0.9 to 0.9, as indicated in the graphs. A missing symbol indicates that the population dropped below its carrying capacity and thus was not analysed. Other parameter values are the same as those indicated in the legend for Table 2. The large arrows indicate the direction of movement of the optimum, and the average rates of optimum movement are the same as those used in Table 2.

selection gradient on trait one for a representative run with steady movement of the optimum. The selection gradient is proportional to the distance of the mean from the optimum (eqn 2), so graphs of β and the lag are virtually identical. Figure 3 provides a baseline against which we can compare the representative runs under the episodic and stochastic models of peak movement, which are shown in Figs 4 and 5, respectively.

The most striking result from the episodic case (Fig. 4) is that the total additive genetic variance experiences cyclical fluctuations in magnitude. These fluctuations are caused by the periodic spikes in the magnitudes of lag and the selection gradient, which occur whenever the peak shifts. Thus, immediately after a peak shift, selection becomes very strong, the population mean responds rapidly and the genetic variance increases. Figure 6 examines these alternating periods of differing selection in more detail. This figure shows the dynamics of the genetic variances and selection gradients, averaged across 20 independent simulation runs, for episodically (with shifts every 100 or 250 generations) and steadily moving optima. In this example, only the optimum for trait one is moving, so trait two experiences mostly stabilizing selection. We can see from Fig. 6 that episodic movement of the optimum results in predictable changes in the genetic variances of both traits. In particular, immediately after a shift in the optimum, the total additive genetic variance in the population increases rapidly. Once the trait mean catches up with the new optimum, however, genetic variation slowly declines. Such surges and declines in genetic variance are more pronounced when the shifts

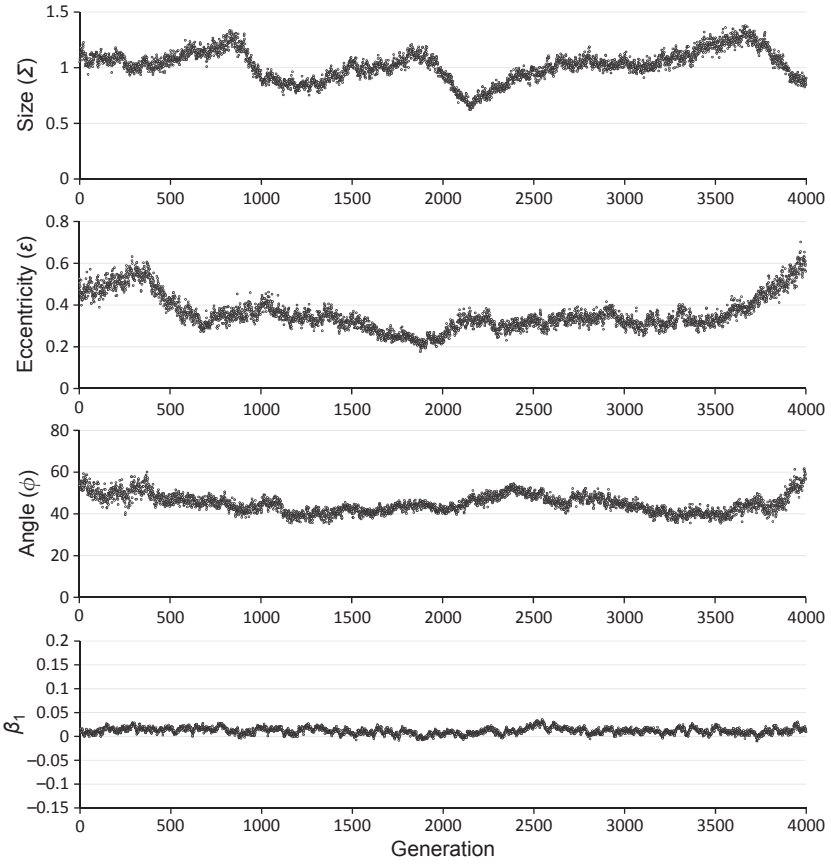

Fig. 3 Data from a simulation run in which the optimum moves steadily over 4000 generations, showing the size (Σ), the inverse measure ε of eccentricity and the angle ϕ of the **G**-matrix, as well as the trait one selection gradient (β_1). In this example, the optimum is moving in a positive direction for both traits (↗), and $\Delta\theta_1 = \Delta\theta_2 = 0.007071$. We assume no selectional correlation ($r_\omega = 0$) and a positive mutational correlation ($r_\mu = 0.5$), which explains the positive angle of **G**. Other parameter values are the same as those for other simulation runs, and their precise values can be found in the Table 2 legend. In this model, directional selection occurs when the population mean is displaced from the optimum, so the value of β_1 is directly proportional to the lag (L_1).

are larger and less frequent (compare Fig. 6a–b). Even though directional selection is only acting on trait one in this example, and mutational and selectional correlations are absent, the additive genetic variance for trait two also varies cyclically due to the pleiotropic effects of the loci (Fig. 6a). This episodic movement of the optimum induces not only distinct cyclical changes in the genetic variances, but also cycles of eccentricity and stability of the angle of the **G**-matrix (Fig. S1).

For a stochastically moving optimum, the situation is quite different (Fig. 5). Stochasticity of the optimum results in larger fluctuations in additive genetic variances (Table S4) that are difficult to discern by inspecting individual simulation runs (Fig. 5). The larger standard deviations in eccentricity and the angle are a bit more obvious (Table S4, Fig. 5), and these differences are attributable to the much larger fluctuations in the selection gradient that occur with a stochastically moving optimum compared with a steadily moving one (compare the bottom panels of Figs 3 and 5).

Effects of episodic and stochastic peak movement on population persistence

Trends in population persistence in changing environments are also apparent in our runs. Because we are interested in comparing genetic variables across simulation runs under different parameter combinations, we stop collecting data when populations drop below their carrying capacities. A drop below the carrying capacity is a step towards population extinction, because populations unable to maintain a stable population size are at a much greater extinction risk than those that invariably remain above their carrying capacities. This assertion is supported by related studies addressing population extinction in response to environmental change (Bürger & Lynch, 1995; Jones, 2008).Our results show that both episodic and stochastic movements of the optimum increase the likelihood that a population will drop below its carrying capacity (Table S5). Such preludes to extinction occur even though the long-term average rate of movement of the optimum is the same as in the steadily moving optimum case. In the case of episodic movement, the effect results from the extremely strong selection imposed immediately after a shift in the optimum. In the case of stochastic movement, the effect results from the tendency for stochasticity to cause the optimum to sometimes move in directions that are misaligned with the genetic line of least resistance. Thus, stochasticity is most costly with respect to population persistence when the **G**-matrix is especially eccentric and when the amount of stochasticity is large (Table S5).

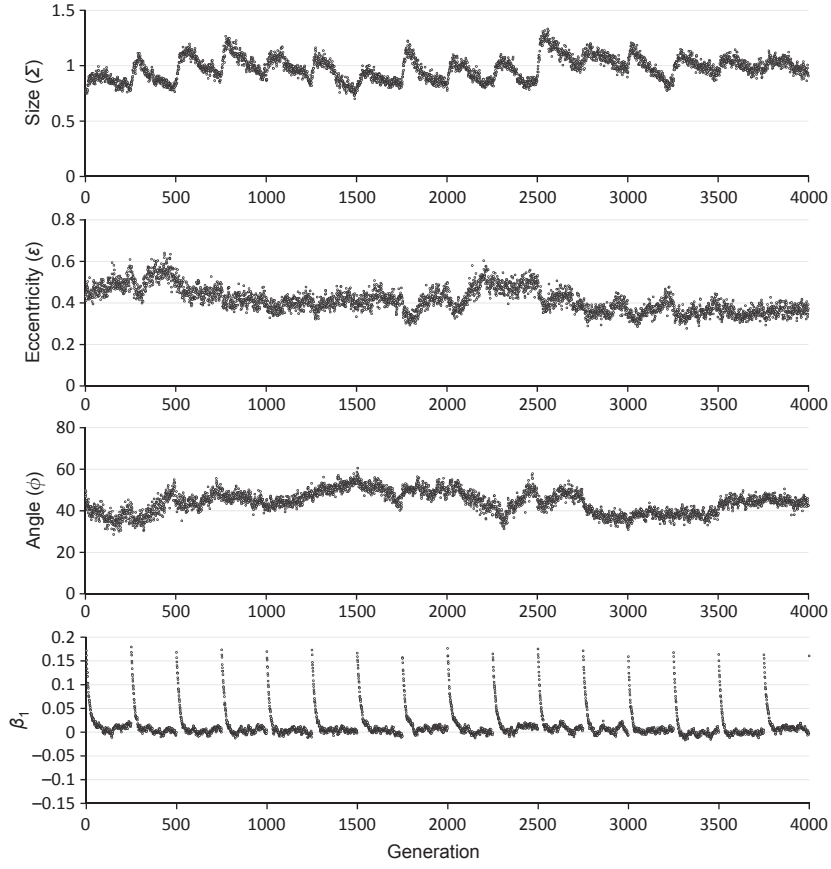

Fig. 4 Data from a simulation run in which the optimum moves episodically over 4000 generations, showing the size (Σ), the inverse measure ε of eccentricity and the angle ϕ of the **G**-matrix, as well as the value of the trait one selection gradient (β_1). In this case, the optimum shifts every 250 generations by an amount 250 times greater per shift than those modelled in Fig. 3. As in Fig. 3, the optimum is moving up and to the right (↗), so each shift results in an increase of 1.768 for the optimum of each trait. This increase is slightly larger than a single phenotypic standard deviation under the parameter values used here. The other parameters for this simulation run are identical to those for Fig. 3. The striking result from episodic movement of the optimum is that the total additive genetic variance shows distinctive cyclical fluctuations (top panel). This pattern is caused by the repeated spikes in the selection gradient (bottom panel).

Peak movement, enhancement of genetic variance and genetic lines of least resistance

In the absence of other constraints, directional selection creates genetic lines of least resistance that facilitate a response to selection by the mean as a result of the aforementioned variance enhancement effect. This effect occurs regardless of the model of peak movement and is apparent from inspection of Tables S1–S3. Figure 7 presents a graphical depiction of these results by showing **G**-matrices under a stationary optimum compared with those under a moving optimum for several different parameter values. We show results for a steadily moving optimum and a stochastically moving optimum, but results from an episodically moving optimum are nearly identical to those from a steadily moving optimum (compare Tables S1 and S2). In the absence of mutational and selectional constraints ($r_\mu = r_\omega = 0$), the **G**-matrix aligns with the direction of peak movement (Fig. 7, upper left). If we include stochasticity in the movement of the optimum (Fig. 7, upper right), we see a slightly larger **G**-matrix that is less well aligned with the direction of peak movement. Finally, when other constraints are present (Fig. 7, bottom panels), the direction of peak movement cannot completely overwhelm these other factors. Nevertheless, even under these conditions, the direction of peak movement still has a major effect on the overall size and shape of the **G**-matrix.

Net-β and the Turelli effect

In Table 3, we present the results of retrospective analysis of selection and calculation of the Turelli effect for the case of a steadily moving optimum. In Table 4, we compare results from the different models of peak movement. Several salient insights can be gleaned from Table 3. One important observation is that the movement of the optimum does not necessarily translate directly into the value of net-**β**. Rather, the relationship between peak movement and the value of net-**β** depends on numerous factors, not the least of which are the values of the mutational and selectional correlations. This nonequivalence between net-**β** and the direction of peak movement is most obvious when the mutational correlation and the selectional correlation are both positive and the optimum moves directly to the right (i.e. $\Delta\theta_1 > 0$, $\Delta\theta_2 = 0$). Even though the optimum for trait two is stationary, the value of net-β_2 is negative, because the

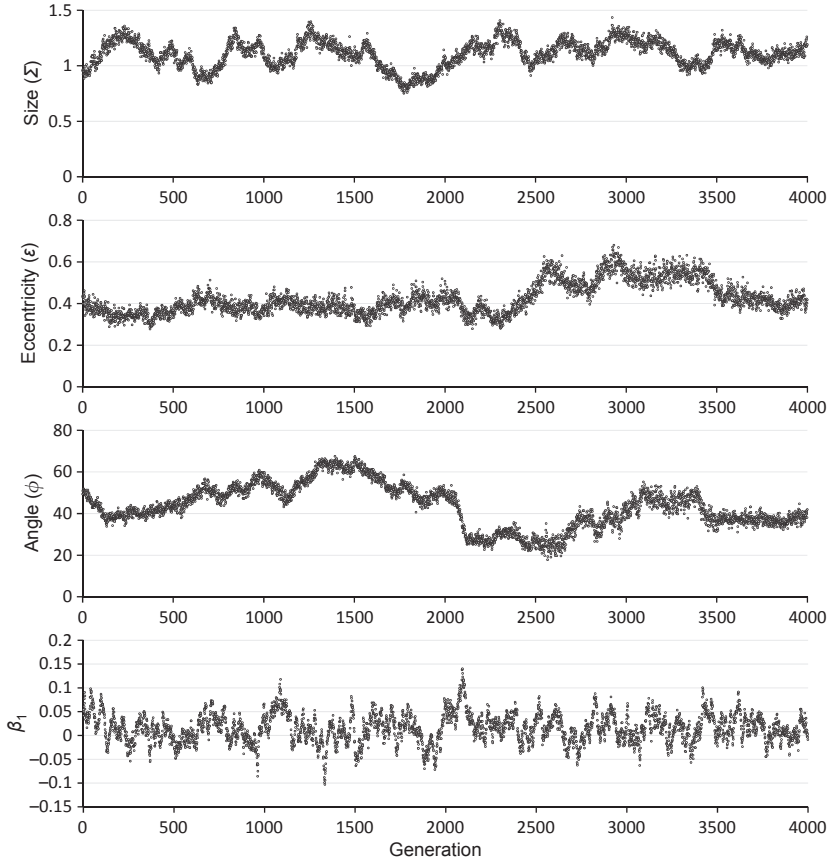

Fig. 5 Data from a simulation run in which the optimum moves stochastically over 4000 generations, showing the size (Σ), the inverse measure ε of eccentricity, and the angle ϕ of the **G**-matrix, as well as the trait one selection gradient (β_1). The parameter values used in this figure are the same as those used for Figs 3 and 4, except in this case the optimum moves every generation at the same average rate as that in Fig. 3 but with an element of stochasticity. In this case, we have $\sigma^2_{\theta 1} = \sigma^2_{\theta 2} = 0.01$. The most obvious patterns here are the highly variable values of the selection gradient (the selection gradient for trait two shows a very similar pattern), and the greater variation in the other variables compared to the steadily moving optimum case (Fig. 3).

positive genetic correlation causes trait two to be displaced from its optimum as trait one responds to its moving optimum.

Perhaps the most disturbing feature of Table 3 is that the values of net-**β** reconstructed by applying eqn (7) substantially underestimate the actual values of net-**β**, as calculated on a generation-by-generation basis according to eqn (2). These underestimates occur whether we reconstruct net-**β** by using the average **G**-matrix (**G**) across the entire simulation run, which would of course never be accessible in an empirical study of evolution covering any appreciable length of evolutionary time, or the **G**-matrix at the end of the simulation run ($\mathbf{G}_T$). The cloud's silver lining is that the angle of the actual net-**β**, which is easily calculated as the arctangent of net-$\boldsymbol{\beta}_2$/net-$\boldsymbol{\beta}_1$, is almost always in close agreement with the angle of the reconstructed net-**β** (Table 3). Thus, even under the parameter values used in this study, which involved relatively strong curvature of the selection surface and a rapidly moving optimum, the reconstruction of net-**β** does a reasonable job of approximating the overall direction of net selection but nearly always underestimates its magnitude (Table 3).

It would be tempting to conclude that the Turelli effect is the cause of the discrepancy between the actual net-**β** and the reconstructed net-**β**, but our results fail to support such a conclusion. Table 3 shows that the Turelli effect does occur (i.e. **G** and **β** covary to some degree), and the sign of the Turelli effect is in the correct direction to partially offset the difference between the actual net-**β** and the reconstructed net-**β**. However, the magnitude of the Turelli effect is too small by approximately an order of magnitude to explain the discrepancy (Table 3).

Analogous results regarding the reconstruction of net-**β** and the Turelli effect hold for episodic and stochastic models of peak movement. In Table 4, we present results for a subset of parameter combinations shown in Table 3 under different models of peak movement. With respect to episodic movement of the optimum, we find that the results are almost identical to those under steady movement (Table 4). However, we do see a very slight tendency for the Turelli effect to be larger in the episodic case. This difference is much smaller than we expected and is not enough to have an appreciable effect on the reconstruction of net-**β**. Under stochastic movement of the optimum, we

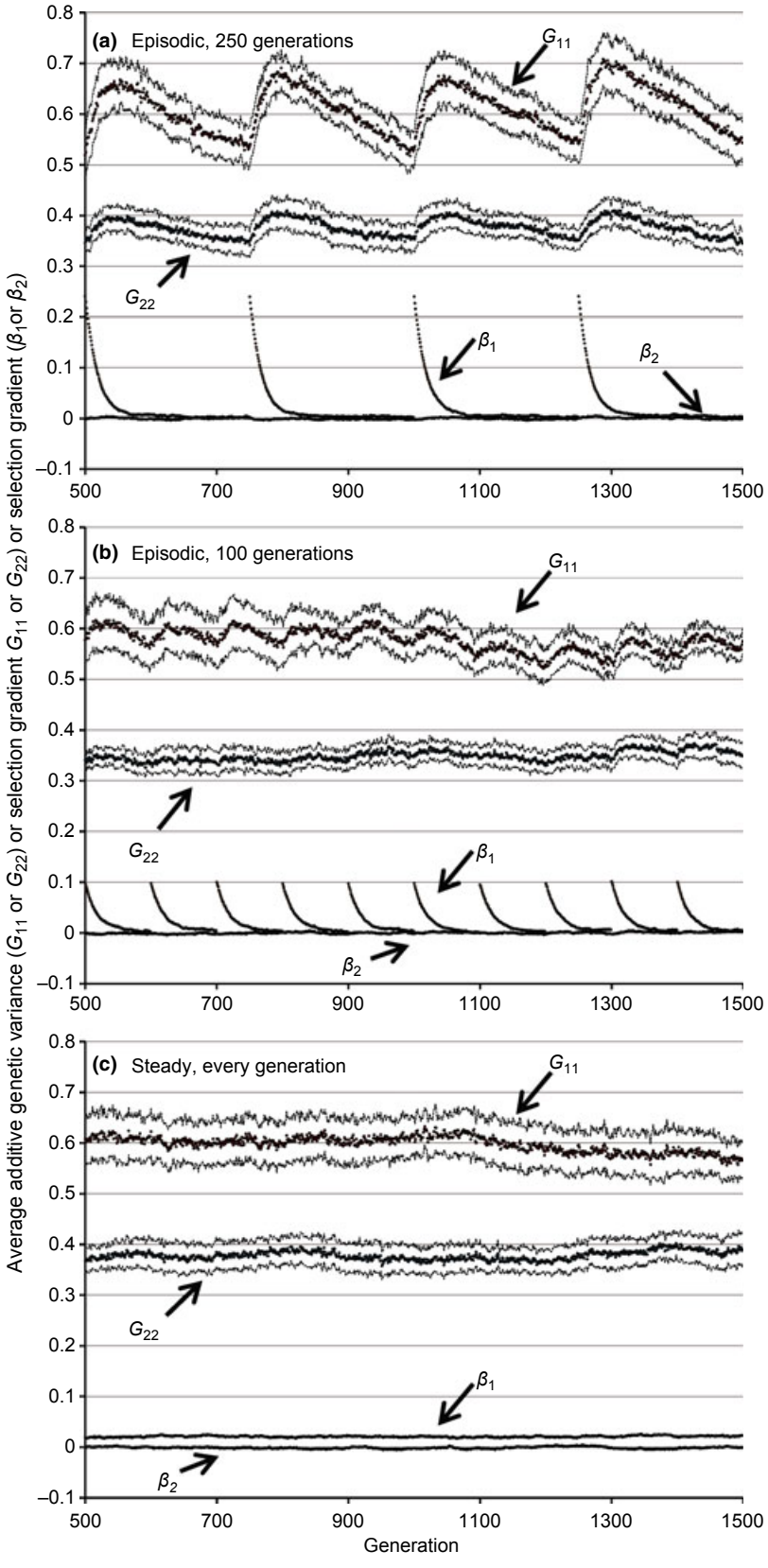

Fig. 6 The effects of episodic peak movement on the additive genetic variance and the selection gradient. Each graph covers 1500 generations of evolution, and each point on the graph is a mean across 20 independent simulation runs. The thin dashed lines surrounding the points for G_{11} and G_{22} represent 95% confidence intervals. The results shown here are those for an optimum moving directly to the right, so the average value of $\Delta\theta_1$ is 0.01 per generation and $\Delta\theta_2$ is held constant at 0. The top two graphs show episodic movement, with the trait one optimum shifting by 2.5 units every 250 generations (a) or 1.0 unit every 100 generations (b). The bottom graph shows results for a steadily moving optimum. This graph illustrates the spikes in the selection gradient (β_1) that occur under episodic peak movement and the increase in genetic variance that occurs as the population evolves towards this new optimum. Also, notice that even though the selection gradient for trait two (β_2) stays near zero, the trait two genetic variance (G_{22}) also shows some cyclical behaviour as a result of pleiotropy. These runs used our core set of parameter values (see Table 2), with $r_\omega = r_\mu = 0$.

find that net-**β** tends to be smaller for the same amount of net movement of the optimum, which is consistent with the higher additive genetic variance maintained under stochastic movement. Otherwise, the discrepancies between the actual net-**β** and the reconstructed net-**β** are still present. The Turelli effect remains small under stochastic movement but becomes unpredictable, as evidenced by the large standard errors in Table 4.

Explaining the discrepancy between reconstructed and actual net-β

Part of the discrepancy between the actual and reconstructed net-**β** can be explained by recalling that the value of **β** is closely related to the lag of the mean phenotype relative to the moving adaptive peak, and the lag may be sensitive to deviations from the assumption of normality of breeding values, as shown by eqns (4) and (6). Assuming a normal distribution of breeding values, the expected lag is given by eqn (3). However, the larger than expected actual values of **β** indicate that the observed lag in our simulations is larger than that predicted by the Gaussian theory.

In Table 5, we present the actual lag for each trait, calculated directly from the observed values in each generation, as well as the expected lag based on eqn (3) or on eqn (6). We apply eqn (3) in two different ways. In the first case, we calculate the expected lag at the end of the run by using the average **G**-matrix in eqn (3). In the second case, we calculate the expected lag on a per-generation basis based on the **G**-matrix for that generation and then average the lag across generations. These calculations show that the expected lag is consistently smaller than the actual lag, indicating that the response to selection is weaker than expected.

Indeed, calculation of the expected lag, **Λ**, based on eqn (6), which takes into account the third moment of the distribution of breeding values, produces a much more accurate estimation of the lag than the estimate based on eqn (3). However, even eqn (6) shows a slight tendency to underestimate the lag, a phenomenon that may be attributable to the Turelli effect or the neglect of even higher moments. The last two columns in Table 5 show that the skewness in the breeding values induced by the moving optimum affects both the estimation of lag and the estimation of **β** to a similar degree, which is to be expected since the lag and **β** are so closely intertwined. In short, our analyses show that estimates of the lag and **β** are affected by the skewness in breeding values, which is caused by directional selection acting on the population. Taking into account the skewness, we achieve a much better estimate of the expected lag (Table 5).

Discussion

This investigation fills a void in our understanding of the evolution of the **G**-matrix by addressing models of peak movement that are more realistic than those used in previous studies. Previous studies addressed stationary peaks (Jones *et al.*, 2003; Guillaume & Whitlock, 2007; Revell, 2007) or peaks that moved at a constant rate in a completely deterministic fashion (Jones *et al.*, 2004). However, real adaptive peaks almost certainly move episodically, and long periods of stasis likely alternate with occasional large jumps (Uyeda *et al.*, 2011). Peak movement probably also includes an additional element of stochasticity, determined by changing community compositions, climatic variation, and other erratic aspects of the environment. Hence, unpredictable generation-to-generation changes in the position of the optimum may belie a long-term directional trend. Our investigation of these more realistic models of peak movement leads to several unexpected insights into the evolutionary dynamics of the **G**-matrix and its response to selection.

Our primary motivation for undertaking this line of research was that previous studies had failed to explore the conditions that seemed especially unfavourable for the stability of the **G**-matrix and the reconstruction of the net selection gradient. *A priori*, we predicted that both episodic and stochastic movement of the optimum would result in less stable **G**-matrices compared with a steadily moving optimum. We also expected that an episodically moving optimum would generate covariance between **G** and **β**, which would result in a large Turelli effect and confound the reconstruction of net-**β** (Shaw *et al.*, 1995; Turelli, 1988). Surprisingly, very few of these predictions were unequivocally supported by our results.

Evolution of the G-matrix under episodic peak movement: the invariance principle

When we consider an episodically moving optimum, one of the most surprising results of our analysis is that the average values of the variables describing the **G**-matrix and the average values of the per-generation changes in these variables are almost the same under an episodically moving optimum as under a steadily moving optimum with the same long-term average rate of movement. In addition, Table S4 shows that the standard deviations of **G**-matrix variables tend to be the same whether the optimum moves steadily or episodically. Even though the average **G**-matrix and the average per-generation changes in the **G**-matrix are the same under an episodically moving optimum as under a steadily moving optimum, we do see some important differences in the evolution of **G** between these modes of peak movement. The most striking difference is that an episodically moving optimum induces predictable,

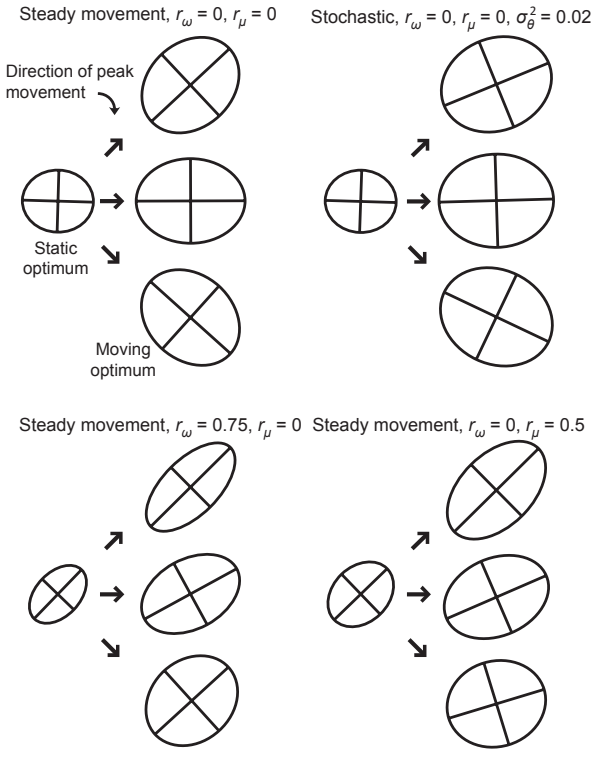

Fig. 7 A visual representation of two important phenomena observed in this study. The first is that a moving optimum increases the total additive genetic variance in the population relative to equilibrium variance when the optimum is stationary. The second phenomenon is that, in the absence of other constraints, a moving optimum causes the **G**-matrix to orient towards the direction of peak movement. Here, we represent the **G**-matrix as a confidence ellipse surrounding 95% of the breeding values in the population (Jones *et al.*, 2004). Thus, larger ellipses represent populations with greater amounts of additive genetic variance, and the long axis of the ellipse shows the direction in phenotypic space that harbours the lion's share of additive genetic variance. The upper left panel shows results for a steadily moving optimum, under the parameter values used for Table 2, except with $r_\omega = r_\mu = 0$. The **G**-matrix on the left is the average **G**-matrix observed under a stationary optimum, the three bold arrows represent the three directions of peak movement, and the three ellipses on the right show the average **G**-matrices that are observed under the corresponding directions of peak movement. Note that in the upper left panel, the average **G**-matrices are larger under a moving optimum and oriented towards the direction of peak movement. The upper right panel shows the results for the same average amount of peak movement, but with stochasticity in the movement of the optimum. Note that the **G**-matrices here are slightly larger and less perfectly oriented compared with those in the upper left panel. Finally, the bottom two panels show results for runs with a positive selectional and mutational correlation, respectively. In these cases, the direction of peak movement can reinforce or oppose the effects of the mutational and selectional correlations on the shape and orientation of the **G**-matrix, depending on whether the direction of peak movement is aligned with the value of the mutational or selectional correlation.

cyclical changes in the **G**-matrix (Figs 4 and 6). In particular, immediately after a major shift in the optimum, the strength of directional selection spikes, and as the population responds to this directional selection, the amount of additive genetic variation in the population increases, only to decrease again once the population reaches the optimum. It is also worth noting that the **G**-matrix increases in eccentricity during the period of directional selection, and the stability of the angle tends to be higher for more eccentric **G**-matrices (Fig. S1). This result is important for the interpretation of the response to selection, because a population that has experienced a recent history of stabilizing selection will provide quantitatively different predictions with respect to its ability to respond to long-term changes in the optimum compared with a population that has experienced a recent history of directional selection.

Evolution of the G-matrix under stochastic movement of the optimum

Stochastic movement of the optimum also has clear effects on the evolution of the **G**-matrix. One of the most obvious and important effects is that stochastic peak movement increases the total additive genetic variance in the population compared with steady or episodic movement (Table 2, Fig. 7). This increase in additive genetic variance, though not large, has the important effect of reducing the average lag in populations evolving in response to a stochastically moving optimum. Thus, the sort of environmental unpredictability that we modelled here seems to favour the maintenance of additive genetic variance.

Another notable difference between the stochastic and deterministic modes of peak movement is that stochastic movement reduces the impact of the direction of peak movement on the evolution of the **G**-matrix. Hence, when the optimum moves in a direction that favours the evolution of an eccentric **G**-matrix with a stable angle under a steadily moving optimum, the addition of stochasticity results in a less eccentric **G**-matrix with a less stable angle. On the other hand, whenever the direction of peak movement produces a highly unstable **G**-matrix under a steadily moving optimum, the addition of stochasticity actually results in a more stable **G**-matrix. Thus, as might be expected, stochasticity in the movement of the optimum ameliorates the effects of optimum movement *per se* on **G**-matrix eccentricity and stability of the angle (Table 2, Fig. 2).

As in the case of an episodically moving optimum, stochasticity has very little effect on the average per-generation changes in most variables describing the **G**-matrix (other than the angle, which it does affect). However, when we consider the standard deviations of these variables across the entire simulation run, we do see significant effects (Table S4). For instance,

Table 3 Results of retrospective analysis of selection under different parameter combinations with steady movement of the optimum ($\sigma^2_{\theta 1} = \sigma^2_{\theta 2} = 0$). The net $\Delta\theta_1$ and $\Delta\theta_2$ columns show the average total distance the optimum moved in units of environmental standard deviation over 4000 generations of evolution. The actual values of net-**β** were calculated by estimating **β** each generation using eqn (2) and summing over generations. Other columns show net-**β** calculated from retrospective selection analysis, from either the mean **G**-matrix ($\bar{\mathbf{G}}$) or the final **G**-matrix at generation 4000 ($\mathbf{G}_T$) using eqn (7). The final two columns show the Turelli effect, **τ**, calculated from eqn (9). All results in this table are means across 20 independent simulation runs. The parameter values not shown are identical to those used in Table 2. The last row shows the mean standard errors (calculated across the 20 simulation runs) of the estimates in each column.

					Actual values			Estimation from $\bar{\mathbf{G}}$			Estimation from $\mathbf{G}_T$			Turelli effect	
r_μ	r_ω	**Δθ**	net $\Delta\theta_1$*	net $\Delta\theta_2$	Net-β_1	Net-β_2	Angle	Net-β_1	Net-β_2	Angle	Net-β_1	Net-β_2	Angle	τ_1	τ_2
0	0	↗	28.3	28.3	62.4	60.2	44.0	48.5	47.1	44.2	47.8	47.2	44.6	−1.7	−1.3
0	0	→	40.0	0.0	85.8	−1.1	−0.7	67.8	−0.5	−0.4	69.3	−0.1	−0.1	−2.3	0.1
0	0	↘	28.3	−28.3	61.9	−61.8	−45.0	48.2	−48.9	−45.4	50.1	−50.4	−45.2	−1.5	1.4
0.5	0	↗	28.3	28.3	51.2	54.7	46.9	40.5	42.2	46.2	42.1	44.6	46.7	−1.1	−1.2
0.5	0	→	40.0	0.0	93.7	−20.9	−12.6	76.7	−22.6	−16.4	79.3	−20.2	−14.3	−2.4	0.7
0.5	0	↘	28.3	−28.3	80.5	−79.6	−44.7	68.0	−68.9	−45.4	68.7	−71.9	−46.3	−2.3	2.0
0	0.75	↗	28.3	28.3	57.9	55.8	43.9	44.3	46.2	46.2	49.9	51.2	45.7	−2.0	−2.0
0	0.75	→	40.0	0.0	119.8	−60.1	−26.6	90.4	−35.9	−21.7	99.1	−38.6	−21.3	−2.9	0.8
0	0.75	↘	28.3	−28.3	109.3	−108.5	−44.8	80.7	−80.9	−45.1	81.0	−84.0	−46.0	−2.4	2.1
0.5	0.75	↗	28.3	28.3	46.2	42.8	42.8	34.0	34.0	45.0	32.6	35.6	47.5	−1.1	−1.3
0.5	0.75	→	40.0	0.0	126.2	−78.1	−31.8	100.5	−59.7	−30.7	99.0	−58.3	−30.5	−2.6	1.5
0.5	0.75	↘	28.3	−28.3	123.6	−124.5	−45.2	100.3	−100.4	−45.0	99.2	−100.8	−45.5	−2.8	3.2
0.5	−0.75	↗	28.3	28.3	101.4	101.0	44.9	73.2	73.5	45.1	77.7	80.3	45.9	−1.6	−2.1
0.5	−0.75	→	40.0	0.0	131.6	35.4	15.1	101.5	9.0	5.1	106.9	9.0	4.8	−3.7	0.5
0.5	−0.75	↘	28.3	−28.3	83.9	−82.3	−44.4	71.9	−69.5	−44.0	68.1	−69.5	−45.6	−3.0	3.0
Mean SE of estimates					1.2	1.3		0.9	0.9		2.9	3.0		0.2	0.2

*Distances of 28.3 and 40.0 environmental standard deviations are equivalent, respectively, to about 23 and 33 phenotypic standard deviations.

Table 4 Results of retrospective analysis of selection under different parameter combinations with episodic or stochastic movement of the optimum. The net $\Delta\theta_1$ and $\Delta\theta_2$ columns show the average total distance the optimum moved in units of environmental standard deviation over 4000 generations of evolution. The values of net-**β** and the Turelli effect, **τ**, are calculated as in Table 3. All results in this table are means across 20 independent simulation runs. Those parameter values not shown are identical to the ones used for Table 2. The standard errors for the variables shown in this table are much smaller than the means (similar to those shown in Table 3), except for the standard errors of some estimates of the Turelli effect. These standard errors are given in parentheses in the last two columns. An entry of "xxx" indicates that some populations dropped below their carrying capacities under the corresponding parameter values and consequently were not analysed.

							Actual values			Estimation from $\bar{\mathbf{G}}$			Estimation from $\mathbf{G}_T$			Turelli effect	
r_μ	r_ω	**Δθ**	Interval	σ^2_θ	Net $\Delta\theta_1$*	Net $\Delta\theta_2$	Net-β_1	Net-β_2	Angle	Net-β_1	Net-β_2	Angle	Net-β_1	Net-β_2	Angle	τ_1 (SEM)	τ_2 (SEM)
0	0	→	1	0	40.0	0.0	85.8	−1.1	−0.7	67.8	−0.5	−0.4	69.3	−0.1	−0.1	−2.3 (0.2)	0.1 (0.1)
0.5	0	→	1	0	40.0	0.0	93.7	−20.9	−12.6	76.7	−22.6	−16.4	79.3	−20.2	−14.3	−2.4 (0.1)	0.7 (0.2)
0	0.75	→	1	0	40.0	0.0	119.8	−60.1	−26.6	90.4	−35.9	−21.7	99.1	−38.6	−21.3	−2.9 (0.2)	0.8 (0.3)
0	0	→	100	0	40.0	0.0	85.9	−0.4	−0.3	68.2	−0.1	−0.1	73.0	0.9	0.7	−2.3 (0.2)	0.1 (0.2)
0.5	0	→	100	0	40.0	0.0	93.6	−22.1	−13.3	76.5	−22.6	−16.5	81.7	−23.4	−16.0	−2.4 (0.2)	1.0 (0.2)
0	0.75	→	100	0	40.0	0.0	121.7	−59.1	−25.9	90.9	−35.3	−21.2	97.4	−41.9	−23.3	−3.1 (0.2)	1.2 (0.2)
0	0	→	250	0	40.0	0.0	85.0	0.2	0.1	66.5	0.8	0.7	84.0	0.6	0.4	−2.8 (0.2)	0.0 (0.2)
0.5	0	→	250	0	40.0	0.0	91.9	−21.4	−13.1	75.1	−22.7	−16.8	81.9	−25.4	−17.2	−2.8 (0.2)	1.2 (0.3)
0	0.75	→	250	0	40.0	0.0	xxx	xxx	xxx	xxx	xxx	xxx	xxx	xxx	xxx	xxx	xxx
0	0	→	1	0.01	40.0	0.0	78.4	−2.1	−1.5	64.9	−1.2	−1.1	72.2	0.6	0.5	0.4 (0.5)	0.3 (0.5)
0.5	0	→	1	0.01	40.0	0.0	87.5	−21.5	−13.8	75.2	−23.1	−17.1	83.3	−25.4	−17.0	1.3 (0.6)	0.2 (0.5)
0	0.75	→	1	0.01	40.0	0.0	104.9	−54.3	−27.4	84.6	−39.8	−25.2	95.7	−48.2	−26.7	3.7 (0.8)	−3.8 (0.9)
0	0	→	1	0.02	40.0	0.0	75.4	−4.0	−3.0	64.8	−2.4	−2.1	66.3	−2.3	−3.0	1.8 (0.3)	1.5 (0.8)
0.5	0	→	1	0.02	40.0	0.0	82.0	−22.5	−15.3	73.3	−23.6	−17.8	77.8	−25.5	−18.1	2.0 (0.8)	1.4 (0.8)
0	0.75	→	1	0.02	40.0	0.0	xxx	xxx	xxx	xxx	xxx	xxx	xxx	xxx	xxx	xxx	xxx

*A distance of 40.0 environmental standard deviations is equivalent to about 33 phenotypic standard deviations.

Table 5 An analysis of the lag under different parameter combinations and directions of peak movement, with steady movement of the optimum. The first three columns indicate the mutational correlation (r_μ), the selectional correlation (r_ω) and the direction of peak movement ($\Delta\boldsymbol{\theta}$), where ↗ means $\Delta\theta_1 = \Delta\theta_2 = 0.0071$, → means $\Delta\theta_1 = 0.01$ and $\Delta\theta_2 = 0$ and ↘ means $\Delta\theta_1 = 0.0071$ and $\Delta\theta_2 = -0.0071$. L_1 and L_2 show the actual lag, which is the observed difference between the optimum and the phenotypic mean, averaged across the 4000 generations. We also show two values of the expected lag under the assumption of Gaussian breeding values. $L_{1,\bar{\mathbf{G}}}$ and $L_{2,\bar{\mathbf{G}}}$ are the expected lag for each trait calculated from eqn (3) using the average **G**-matrix from the simulation run. $L_{1,\mathbf{G}(t)}$ and $L_{2,\mathbf{G}(t)}$ are also expected lags based on eqn (3), but in this case they are calculated by applying eqn (3) each generation and averaging across the values of expected lag calculated each generation. We also present the expected lag based on eqn (6), which relaxes the Gaussian assumption. We apply the equation every generation and average across the 4000 experimental generations. These values are $\Lambda_{1,\mathbf{G}(t)}$ and $\Lambda_{2,\mathbf{G}(t)}$. The penultimate column shows the ratio of the expected lag for trait one with the assumption of Gaussian breeding values to that without the Gaussian assumption. The final column shows the ratio of the reconstructed net-β_1 to the actual net-β_1 (from Table 4), illustrating that the skewness affecting the expected lag also largely accounts for the underestimation of net-$\boldsymbol{\beta}$. The data shown in this table are from the same simulation runs as those used for Table 4. The last row shows the mean standard errors of each column.

r_μ	r_ω	$\Delta\boldsymbol{\theta}$	L_1	L_2	$L_{1,\bar{\mathbf{G}}}$	$L_{2,\bar{\mathbf{G}}}$	$L_{1,\mathbf{G}(t)}$	$L_{2,\mathbf{G}(t)}$	$\Lambda_{1,\mathbf{G}(t)}$	$\Lambda_{2,\mathbf{G}(t)}$	$\frac{L_{1,\bar{\mathbf{G}}}}{\Lambda_{1,\mathbf{G}(t)}}$	$\frac{\beta_{1,\bar{\mathbf{G}}}}{\beta_{1,\text{actual}}}$
0	0	↗	0.165	0.159	0.128	0.125	0.133	0.129	0.159	0.154	0.81	0.82
0	0	→	0.227	−0.003	0.180	−0.001	0.186	−0.001	0.219	−0.002	0.82	0.84
0	0	↘	0.164	−0.163	0.127	−0.129	0.131	−0.133	0.157	−0.158	0.81	0.82
0.5	0	↗	0.137	0.146	0.108	0.112	0.111	0.116	0.135	0.141	0.80	0.87
0.5	0	→	0.246	−0.052	0.202	−0.056	0.208	−0.059	0.239	−0.050	0.84	0.87
0.5	0	↘	0.209	−0.207	0.177	−0.180	0.184	−0.186	0.203	−0.202	0.87	0.87
0	0.75	↗	0.248	0.246	0.196	0.198	0.205	0.206	0.241	0.241	0.81	0.82
0	0.75	→	0.211	0.051	0.175	0.063	0.181	0.066	0.205	0.051	0.86	0.79
0	0.75	↘	0.100	−0.096	0.072	−0.073	0.074	−0.075	0.095	−0.090	0.76	0.77
0.5	0.75	↗	0.197	0.194	0.150	0.149	0.155	0.155	0.192	0.190	0.78	0.80
0.5	0.75	→	0.196	0.017	0.161	0.020	0.165	0.021	0.188	0.016	0.85	0.83
0.5	0.75	↘	0.107	−0.111	0.088	−0.089	0.090	−0.092	0.101	−0.105	0.87	0.83
0.5	−0.75	↗	0.093	0.091	0.066	0.068	0.067	0.070	0.087	0.088	0.76	0.76
0.5	−0.75	→	0.282	−0.132	0.249	−0.149	0.260	−0.158	0.278	−0.134	0.89	0.81
0.5	−0.75	↘	0.357	−0.355	0.303	−0.301	0.317	−0.315	0.353	−0.351	0.86	0.88
Mean SE of estimates			0.003	0.003	0.002	0.002	0.002	0.002	0.003	0.003		

a stochastically moving optimum results in a large increase in the standard deviations of the additive genetic variances and the eccentricity of the **G**-matrix. Thus, these results support the notion that stochastic movement of the optimum results in a less stable **G**-matrix.

Increased G-matrix stability via the variance enhancement effect

Another key result, which occurs regardless of the model of peak movement, is that directional selection alone, in the absence of mutational or selectional correlations, promotes **G**-matrix stability (Table 2, Fig. 7). The stability-conferring effects of peak movement are caused by the tendency of a moving peak to result in a higher equilibrium level of additive genetic variance compared to a stationary peak, in particular in the direction of the moving peak. An increase in genetic variation under various forms of directional selection has been observed previously, both for a single trait (Barton & Turelli, 1987; Bürger, 1993; Bürger & Lynch, 1995) and for two pleiotropically coupled traits (Jones *et al.*, 2004). This increase in variance requires sufficiently large population size and is apparently due to recurrent favourable mutations sweeping towards fixation (Bürger, 2000; Chap. VII.7; see also Turelli, 1985; Wagner, 1989; Baatz & Wagner, 1997). The genetic basis of the adaptation of a univariate trait to a moving optimum, especially with respect to the properties of the selective sweeps and the distribution of the substitutions, is addressed in detail by Kopp & Hermisson (2009a,b).An important point is that this variance enhancement effect compares the effects of directional selection (caused by a moving peak) to the effects of stabilizing selection (under a stationary peak) rather than to expectations under neutrality. Although the variance observed under a moving optimum is higher than that under pure stabilizing selection, it is always lower than under (neutral) mutation–drift balance (Lynch & Hill, 1986; Bürger & Lynch, 1995).

An evolving G-matrix, the net selection gradient and the Turelli effect

Our results provide some novel perspectives regarding the effects of selection over long periods of evolutionary time. Two results of the present analysis appear to be especially important and general. The first result is the one just discussed: the movement of the optimum causes an increase in additive genetic variation in the direction of optimum movement, which in turn

facilitates a response to selection by the trait mean. The second result is that, because the mean lags behind the optimum, selection causes the distribution of breeding values to become skewed in the direction of peak movement, a situation that actually retards a response to selection by the mean. These two opposing phenomena do not precisely offset one another, so both must be considered in the reconstruction of net-**β**. Unfortunately, no simple method exists to correct estimates of net-**β** in the light of these issues, because the magnitude of each effect appears to depend on a wide range of factors. Nevertheless, awareness of the issues will at least lead to caution in interpretation of the history (or future) of the response to selection in any given system.

Of course, the most convenient way to estimate Lande's net selection gradient is to assume a constant **G**-matrix (Price & Grant, 1985; Arnold, 1988; Merilä *et al.*, 1994; Cheverud, 1996; Dudley, 1996), but our results show that such an approach may only give a rough approximation of the history of peak movement experienced by a lineage. The most troubling observation in our current study with respect to net-**β** is that directional selection can result in skewed breeding values, which makes the Gaussian approximation inaccurate. When we use the Gaussian assumptions for the expected lag and net-**β**, we find that both coordinates deviate from the actual values, often by 20% or more. In particular, populations lag farther behind the optimum than expected, and a stronger **β** than expected is required to produce the observed response to selection (Tables 3–5). If we estimate the expected lag based on theory that takes into account the skewness in breeding values (eqn (6) and Appendix I), however, we find that the expected lag much more closely approaches the actual lag, confirming that this skewness is the major source of discrepancy between expectations under the Gaussian theory and observed values.

Despite the fact that selection induces skewness in breeding values, the reconstruction of a meaningful net-**β** may still be possible. One encouraging observation is that, even though the values of net-**β** were quite far from the mark in terms of magnitude, the angle of the reconstructed net-**β** was usually close to the true angle. A second encouraging observation is that on a selection surface with less curvature (i.e. $\omega_{11} = \omega_{22} = 49$), Jones *et al.* (2004) found that the reconstructed net-**β** was very close to the actual net-**β**, suggesting that the skewness problem applies to a lesser extent when stabilizing selection is weak, a conclusion which is also supported by analytical theory. Finally, as we have shown in Table 5, the ratio of the expected value of lag under the Gaussian assumption to the expected value of lag taking into account the skewness is similar to the ratio of the reconstructed net-**β** to the true net-**β**. This observation implies that the discrepancy between the expected lag calculated using eqn (3) and that calculated from eqn (6) can provide a rough idea of how far the reconstructed net-**β** differs from the actual net-**β**, assuming the present skewness in the phenotypic distribution is representative of the skewness in breeding values over the time frame of interest.

The final point of relevance to the reconstruction of net-**β** concerns the Turelli effect. We expected an episodically moving optimum to result in a much higher covariance between **G** and **β** compared with a steadily moving optimum, which would result in much larger values of the Turelli effect, further compromising the estimation of net-**β**. Contrary to our expectations, the Turelli effect is small relative to the value of **β** under all models of peak movement. Episodic peak movement appears to result in a very small increase in the Turelli effect relative to steady peak movement (Table 4), but the absolute value of the Turelli effect remains < 3% the value of net-**β**. Under a stochastically moving optimum, the Turelli effect also is small, but is much more variable among runs. Thus, we conclude that, compared with skewed breeding values, the Turelli effect is not a major problem for the reconstruction of net-**β** under most realistic models of peak movement.

The model of peak movement and population persistence

We found that episodically and stochastically moving optima increase the probability that a population will drop below its carrying capacity relative to a population that experiences a stationary optimum or a peak that moves steadily in a single direction. A population can persist in a changing environment when the trait mean is able to evolve at a rate that is at least as fast as the rate at which the optimum moves (Lynch & Lande, 1993; Bürger & Lynch, 1995). When the optimum moves a large distance in a single generation, the entire population will experience a sudden drop in average fitness that can be dramatic enough to prevent the population from being able to produce enough surviving offspring to remain above the carrying capacity. Furthermore, when the optimum moves stochastically, it will sometimes move in a direction that crosses genetic lines of least resistance. Under these circumstances, the population may have insufficient additive genetic variance in the direction of the optimum shift to evolve towards its new location. This situation is most likely to arise when genetic correlations are strong, because the eccentricity of the **G**-matrix will then be a major constraint. Thus, we conclude that both episodic and stochastic models of peak movement are more likely to cause a population to drop below its carrying capacity and by extension face a heightened risk of extinction, compared to a population with a steadily, deterministically moving optimum.

Limitations and conclusions

The type of simple model employed here has some limitations, and future work correcting some of these shortcomings could pay dividends. One of the major features of our model is the assumption of only additive genetic effects. This limitation is partially a modelling convenience, because restricting the model to additive effects results in a number of favourable features related to the estimation of the **G**-matrix and interpretation in the light of existing theory. However, real systems probably include substantial components of dominance and epistasis, so future studies could profitably explore these more complicated models of inheritance. In addition, many of our most important results probably rely heavily on the way we model mutations. We assume a Gaussian distribution of mutational effects and that mutants have no pleiotropic deleterious side effects. Mutational effects could in principle follow a more leptokurtic pattern in which major mutations sometimes occur (see e.g. Zhang & Hill, 2003) or mutations could be mostly deleterious (Zhang *et al.*, 2004), a situation that would certainly affect our results. We also make a number of other assumptions, such as an exceptionally high mutation rate, which are discussed in some detail in previous papers (Jones *et al.*, 2003, 2004). Future models, incorporating more realistic assumptions regarding mutation rates and mutational effects, will no doubt shed additional light on the issues addressed in the present study.

In conclusion, our results shed new light on aspects of **G**-matrix evolution under more realistic models of movement of the optimum than have heretofore been explored. Our results provide new insights into general effects of the operation of selection, the maintenance of genetic variation, the reconstruction of net-**β** and the effects of peak movement on population persistence. Although these results appear to make the already complex study of selection even more difficult, our simulations uncover several generalizations that simplify our understanding of how peak movement affects the evolution of both the multivariate mean and the **G**-matrix.

Acknowledgments

This work was supported by funding from the National Science Foundation (grant DEB-0447854 to S.J.A. and R.B. and grant DEB-0448268 to A.G.J.), the Austrian Science Fund FWF (grant P21305 to R.B.), a National Institutes of Health Ruth L. Kirschstein National Research Service Award (5F32G-M076995) to P.A.H., and a NSF Graduate Research Fellowship to J.C.U. Additional support for P.A.H. was also provided by NIH/NCRR grant P20RR16448 to L. Forney.

References

Arnold, S.J. 1988. Quantitative genetics and selection in natural populations: microevolution of vertebral numbers in the garter snake *Thamnophis elegans*. In: *Proceedings of the Second International Conference on Quantitative Genetics* (B.S. Weir, E.J. Eisen, M.M. Goodman & G. Namkoong, eds), pp. 619–636. Sinauer, Sunderland, MA.

Arnold, S.J., Pfrender, M.E. & Jones, A.G. 2001. The adaptive landscape as a conceptual bridge between micro- and macroevolution. *Genetica* **112**: 9–32.

Arnold, S.J., Bürger, R., Hohenlohe, P.A., Ajie, B.C. & Jones, A.G. 2008. Understanding the evolution and stability of the **G**-matrix. *Evolution* **62**: 2451–2461.

Baatz, M. & Wagner, G.P. 1997. Adaptive inertia caused by hidden pleiotropic effects. *Theor. Pop. Biol.* **51**: 49–66.

Barton, N.H. & Turelli, M. 1987. Adaptive landscapes, genetic distance, and the evolution of quantitative characters. *Genet. Res.* **49**: 157–174.

Bürger, R. 1991. Moments, cumulants, and polygenic dynamics. *J. Math. Biol.* **30**: 199–213.

Bürger, R. 1993. Predictions of the dynamics of a polygenic character under directional selection. *J. Theor. Biol.* **162**: 487–513.

Bürger, R. 2000. *The Mathematical Theory of Selection, Recombination, and Mutation*. John Wiley & Sons, Chichester.

Bürger, R. & Lande, R. 1994. On the distribution of the mean and variance of a quantitative trait under mutation-selection-drift balance. *Genetics* **138**: 901–912.

Bürger, R. & Lynch, M. 1995. Evolution and extinction in a changing environment: a quantitative-genetic analysis. *Evolution* **49**: 151–163.

Bürger, R., Wagner, G.P. & Stettinger, F. 1989. How much heritable variation can be maintained in finite populations by mutation-selection balance? *Evolution* **43**: 1748–1766.

Cheverud, J.M. 1996. Quantitative genetic analysis of cranial morphology in the cotton-top (*Saguinus oedipus*) and saddleback (*S. fuscicollis*) tamarins. *J. Evol. Biol.* **9**: 5–42.

Crow, J.F. & Kimura, M. 1964. The theory of genetic loads. In: *Proceedings of the XI International Congress of Genetics* (S.J. Geerts, ed.), pp. 495–505. Pergamon, Oxford, UK.

Dudley, S.A. 1996. The response to differing selection on plant physiological traits: evidence for local adaptation. *Evolution* **50**: 103–110.

Estes, S. & Arnold, S.J. 2007. Resolving the paradox of stasis: models with stabilizing selection explain evolutionary divergence on all timescales. *Am. Nat.* **169**: 227–244.

Gingerich, P.D. 2001. Rates of evolution on the time scale of the evolutionary process. *Genetica* **112/113**: 127–144.

Guillaume, F. & Whitlock, M.C. 2007. Effects of migration on the genetic covariance matrix. *J. Evol. Biol.* **61**: 2398–2409.

Jones, A.G. 2008. A theoretical quantitative genetic study of negative ecological interactions and extinction times in changing environments. *BMC Evol. Biol.* **8**: 119.

Jones, A.G., Arnold, S.J. & Bürger, R. 2003. Stability of the **G**-matrix in a population experiencing pleiotropic mutation, stabilizing selection, and genetic drift. *Evolution* **57**: 1747–1760.

Jones, A.G., Arnold, S.J. & Bürger, R. 2004. Evolution and stability of the **G**-matrix on a landscape with a moving optimum. *Evolution* **58**: 1639–1654.

Jones, A.G., Arnold, S.J. & Bürger, R. 2007. The mutation matrix and the evolution of evolvability. *Evolution* **61**: 727–745.

Kinnison, M.T. & Hendry, A.P. 2001. The pace of modern life. II. From rates of contemporary microevolution to pattern and process. *Genetica* **112/113**: 145–164.
Kopp, M. & Hermisson, J. 2009a. The genetic basis of phenotypic adaptation I: fixation of beneficial mutations in the moving optimum model. *Genetics* **182**: 233–249.
Kopp, M. & Hermisson, J. 2009b. The genetic basis of phenotypic adaptation II: the distribution of adaptive substitutions in the moving optimum model. *Genetics* **183**: 1453–1476.
Lande, R. 1979. Quantitative genetic analysis of multivariate evolution, applied to brain:body size allometry. *Evolution* **33**: 402–416.
Lynch, M. & Hill, W.G. 1986. Phenotypic evolution by neutral mutation. *Evolution* **40**: 915–935.
Lynch, M. & Lande, R. 1993. Evolution and extinction in response to environmental change. In: *Biotic Interactions and Global Change* (P. Kareiva, J. Kingsolver & R. Huey, eds), pp. 234–250. Sinauer Associates, Sunderland, MA.
Merilä, J., Björklund, M. & Gustafsson, L. 1994. Evolution of morphological differences with moderate genetic correlations among traits as exemplified by two flycatcher species (*Ficedula*; Muscicapidae). *Biol. J. Linn. Soc.* **52**: 19–30.
Price, T.D. & Grant, P.R. 1985. The evolution of ontogeny in Darwin's finches: a quantitative genetic approach. *Am. Nat.* **125**: 169–188.
Revell, L.J. 2007. The **G** matrix under fluctuating correlational mutation and selection. *Evolution* **61**: 1857–1872.
Schluter, D. 1996. Adaptive radiation along genetic lines of least resistance. *Evolution* **50**: 1766–1774.
Shaw, F.H., Shaw, R.G., Wilkinson, G.S. & Turelli, M. 1995. Changes in genetic variances and covariances: **G** whiz! *Evolution* **49**: 1260–1267.
Steppan, S.J., Phillips, P.C. & Houle, D. 2002. Comparative quantitative genetics: evolution of the **G** matrix. *Trends Ecol. Evol.* **17**: 320–327.
Turelli, M. 1985. Effects of pleiotropy on predictions concerning mutation-selection balance for polygenic traits. *Genetics* **111**: 165–195.
Turelli, M. 1988. Phenotypic evolution, constant covariances, and the maintenance of additive variation. *Evolution* **42**: 1342–1347.
Turelli, M. & Barton, N.H. 1990. Dynamics of polygenic characters under selection. *Theor. Pop. Biol.* **38**: 1–57.
Turelli, M. & Barton, N.H. 1994. Genetic and statistical analyses of strong selection on polygenic traits: what, me normal? *Genetics* **138**: 913–941.
Uyeda, J.C., Hansen, T.F., Arnold, S.J. & Peinaar, J. 2011. The million-year wait for macroevolutionary bursts. *Proc. Natl. Acad. Sci. USA* **108**: 15908–15913.
Wagner, G.P. 1989. Multivariate mutation-selection balance with constrained pleiotropic effects. *Genetics* **122**: 223–234.
Yeaman, S. & Guillaume, F. 2009. Predicting adaptation under migration load: the role of genetic skew. *Evolution* **63**: 2926–2938.
Zhang, X. S. & Hill, W. G. 2003. Multivariate stabilizing selection and pleiotropy in the maintenance of quantitative genetic variation. *Evolution* **57**: 1761–1775.
Zhang, X.S., Wang, J.L. & Hill, W.G. 2004. Influence of dominance, leptokurtosis and pleiotropy of deleterious mutations on quantitative genetic variation at mutation-selection balance. *Genetics* **166**: 597–610.

Appendix 1: Multivariate selection response and lag with skewed breeding values

Our aim here is to derive the response to general selection of the mean vector of breeding values of a multivariate trait without making assumptions on the distribution of breeding values. Then, we shall apply this equation to derive the response to selection and the lag for the moving optimum model used in the main text.

We consider I traits, and the trait values of individuals are given by $z_1 = x_1 + e_1$, $z_2 = x_2 + e_2$, …,$z_I = x_I + e_I$. Thus, each individual is characterized by a column vector of trait values ($\mathbf{z}$), a column vector of genotypic (i.e. breeding) values ($\mathbf{x}$) and a column vector of environmental effects ($\mathbf{e}$). Let $W(\mathbf{z})$ denote the fitness of individuals of phenotype $\mathbf{z}$, and $w(\mathbf{x})$ the (average) fitness of individuals of genotypic values $\mathbf{x}$. Then, clearly, the mean fitness satisfies $\overline{W} = \bar{w}$. If $P(\mathbf{x})$ denotes the distribution of breeding values, the exact change in the distribution of breeding values caused by selection is

$$\Delta_s P(\mathbf{x}) = P(\mathbf{x})(w(\mathbf{x}) - \overline{W})/\overline{W}. \tag{A.1}$$

We follow the approach devised by Bürger (1991) and Turelli & Barton (1994) and use cumulants and higher-order selection differentials to derive the multivariate selection response of the mean. Denoting the moment-generating function of $P(\mathbf{x})$ by $\Psi(\boldsymbol{\xi})$ and the cumulant-generating function by $\Phi(\boldsymbol{\xi}) = \ln(\Psi(\boldsymbol{\xi}))$, the response to selection in terms of generating functions (Turelli & Barton, 1994; Bürger, 2000, p. 174) is

$$\Delta_s \Psi(\boldsymbol{\xi}) = \int \Gamma(\boldsymbol{\xi}, \boldsymbol{\eta}) \frac{\partial \ln \overline{W}}{\partial \Phi(\boldsymbol{\eta})} \mathrm{d}\boldsymbol{\eta}, \tag{A.2}$$

where $\Gamma(\boldsymbol{\xi}, \boldsymbol{\eta}) = \exp\,[\Psi(\boldsymbol{\xi} + \boldsymbol{\eta}) - \Psi(\eta)] - \exp\,[\Psi(\boldsymbol{\xi})]$

We denote the multivariate cumulants of order 1, 2, 3, 4, … of the (multivariate) distribution of breeding values by κ_i, κ_{ij}, κ_{ijk}, κ_{ijkl}, …, respectively. The first-order cumulants are just single-trait means, the second-order cumulants are the genetic variances and covariances, and the third-order cumulants are the third-order central moments, that is,

$$\kappa_i = \bar{x}_i, \quad \kappa_{ij} = G_{ij}, \quad \kappa_{ijk} = \int (x_i - \bar{x}_i)(x_j - \bar{x}_j)(x_k - \bar{x}_k)\mathrm{d}x. \tag{A.3}$$

Of course, i, j and k need not be different and the order is irrelevant, thus $\kappa_{iij} = \kappa_{iji} = \kappa_{jii}$.

The response $\Delta_s \bar{x}_i$ of the mean of trait i is obtained by differentiating (eqn A.2) once with respect to ξ_i. Paraphrasing the derivation of eqn (17a) in Turelli & Barton

(1994) and specifying their formula to $U = \{i\}$(and $V = \{i, j, k, \ldots,\}$) produce the fundamental equation for the selection response of the mean:

$$\Delta_s \bar{x}_i = \sum_{j=1}^{I} \kappa_{ij} \frac{\partial \ln \overline{W}}{\partial \kappa_j} + \sum_{j,k=1}^{I} \kappa_{ijk} \frac{\partial \ln \overline{W}}{\partial \kappa_{jk}} + \sum_{j,k,l=1}^{I} \kappa_{ijkl} \frac{\partial \ln \overline{W}}{\partial \kappa_{jkl}} + \cdots. \quad (A.4)$$

Because recombination, symmetric mutation, random mating and random genetic drift do not alter the means (e.g. Bürger, 2000), the response of the means across generations is also given by eqn (A.4), that is $\Delta \bar{x}_i = \Delta_s \bar{x}_i$.

In principle, the above approach could be generalized to derive the response to selection of the variances, covariances and higher cumulants of the distribution of breeding values. However, as already envisaged in the univariate case (Turelli & Barton, 1994; Bürger, 2000), this leads to enormous complications because not only the effects of recombination and genetic drift have to be taken into account, but also genetic details, such as number of loci and distribution of allelic effects at each locus, influence the evolutionary dynamics of the cumulants of order > 1.

Now we apply eqn (A.3) to our model. Assuming weak selection, we can approximate the fitness of individuals with vector $\mathbf{x}$ of genotypic values by

$$w(\mathbf{x}) = 1 - \frac{1}{2}(\mathbf{x} - \boldsymbol{\theta})^T \boldsymbol{\Omega}^{-1} (\mathbf{x} - \boldsymbol{\theta}). \quad (A.5)$$

Here, $\boldsymbol{\Omega}$ is a matrix that describes the curvature of the fitness landscape for breeding values, and $\boldsymbol{\theta}$ is the position of the optimum. We write a_{ij} for the entries of the $I \times I$ matrix $\boldsymbol{\Omega}^{-1}$. In the notation of the main text, $\boldsymbol{\Omega} = \boldsymbol{\omega} + \mathbf{E}$. Then

$$\begin{aligned} \overline{W} &\approx 1 - \frac{1}{2} \sum_{i,j} a_{ij} \left[(\bar{x}_i - \theta_i)(\bar{x}_j - \theta_j) + G_{ij} \right] \\ &= 1 - \frac{1}{2} \sum_{i,j} a_{ij} G_{ij} - \frac{1}{2} (\bar{\mathbf{x}} - \boldsymbol{\theta})^T \boldsymbol{\Omega}^{-1} (\bar{\mathbf{x}} - \boldsymbol{\theta}), \end{aligned} \quad (A.6)$$

From eqn (A.4) and because all partial derivatives of $\overline{W}$ with respect to cumulants of order higher than two vanish, the response of the genotypic means to selection is given by

$$\Delta \bar{x}_i \approx \sum_{j=1}^{I} G_{ij} \frac{\partial \overline{W}}{\partial \bar{x}_j} + \sum_{j,k=1}^{I} \kappa_{ijk} \frac{\partial \overline{W}}{\partial G_{jk}}. \quad (A.7)$$

This formula is approximate only because we assumed weak selection.

To present eqn (A.7) in instructive vector form, we write

$$\nabla_{\bar{\mathbf{x}}} \overline{W} = \left(\frac{\partial \overline{W}}{\partial \bar{x}_1}, \ldots, \frac{\partial \overline{W}}{\partial \bar{x}_I} \right)^T, \quad (A.8)$$

which is the classical selection gradient, and

$$\nabla_{\mathbf{G}} \overline{W} = \left(\frac{\partial \overline{W}}{\partial G_{11}}, \ldots, \frac{\partial \overline{W}}{\partial G_{II}} \right)^T, \quad (A.9)$$

which is the second-order selection gradient (see above) and a vector of length I^2. Finally, we define the $I \times I^2$ matrix

$$\mathbf{C} = \begin{pmatrix} \kappa_{111} & \kappa_{112} & \cdots & \kappa_{11I} & \cdots & \cdots & \kappa_{1I1} & \kappa_{1II} \\ \kappa_{211} & \kappa_{212} & \cdots & \kappa_{21I} & \cdots & \cdots & \kappa_{2I1} & \kappa_{2II} \\ \vdots & \vdots & & \vdots & & & \vdots & \vdots \\ \kappa_{I11} & \kappa_{I12} & \cdots & \kappa_{I1I} & \cdots & \cdots & \kappa_{II1} & \kappa_{III} \end{pmatrix}. \quad (A.10)$$

Now we can cast (A.7) in matrix form:

$$\Delta \bar{\mathbf{x}} \approx \mathbf{G} \nabla_{\bar{\mathbf{x}}} \overline{W} + \mathbf{C} \nabla_{\mathbf{G}} \overline{W}. \quad (A.11)$$

Simple calculations show that

$$\frac{\partial \overline{W}}{\partial \bar{x}_j} = -\sum_k a_{jk} (\bar{x}_k - \theta_k), \quad (A.12)$$

$$\frac{\partial \overline{W}}{\partial G_{jk}} = -\frac{1}{2} a_{jk}. \quad (A.13)$$

From now on, we assume a constantly moving optimum, such that $\boldsymbol{\theta}(t) = t\Delta\boldsymbol{\theta}$, where t is time in generations and $\Delta\boldsymbol{\theta}$ represents the amount the optimum moves per generation. If the expected lag is defined as $\Lambda = \boldsymbol{\theta} - \bar{\mathbf{x}}$, then (A.12) yields

$$\nabla_{\bar{\mathbf{x}}} \overline{W} = \boldsymbol{\Omega}^{-1} \Lambda. \quad (A.14)$$

Because for a constantly moving optimum, we must have $\Delta\mathbf{x} = \Delta\boldsymbol{\theta}$, a simple calculation invoking (A.11) produces

$$\Lambda \approx \boldsymbol{\Omega} \mathbf{G}^{-1} \left(\Delta\boldsymbol{\theta} - \mathbf{C} \nabla_{\mathbf{G}} \overline{W} \right). \quad (A.15)$$

We use this equation in the main text, but use slightly different notation for $\mathbf{C}$ for the sake of clarity. In the two-trait case,

$$\mathbf{C} = \begin{pmatrix} \kappa_{111} & \kappa_{112} & \kappa_{121} & \kappa_{122} \\ \kappa_{211} & \kappa_{212} & \kappa_{221} & \kappa_{222} \end{pmatrix} = \begin{pmatrix} c_{3,0} & c_{2,1} & c_{2,1} & c_{1,2} \\ c_{2,1} & c_{1,2} & c_{1,2} & c_{0,3} \end{pmatrix}, \quad (A.16)$$

where $c_{i,j} = \int (x_1 - \bar{x}_1)^i (x_2 - \bar{x}_2)^j P(\mathbf{x}) d\mathbf{x}$.

The attentive reader may note that in the absence of skew, (eqn A.14) and (4) differ slightly from the Gaussian prediction (3) because $\boldsymbol{\omega} + \mathbf{P} \neq \boldsymbol{\Omega}$. The reason is that the derivation of eqn (A.14) assumes weak selection, which is not assumed in deriving (3). Clearly, under weak selection, $\boldsymbol{\omega} + \mathbf{P} = \boldsymbol{\Omega} + \mathbf{G} \approx \boldsymbol{\Omega}$.

Supporting information

Additional Supporting Information may be found in the online version of this article:

Table S1 Mean values of population-level genetic variables and per-generation changes in these variables for an optimum that moves steadily, that is, the optuimum moves every generation by a small amount.

Table S2 Mean values of population-level genetic variables and per-generation changes in these variables for an episodically moving optimum.

Table S3 Mean values of population-level genetic variables and per-generation changes in these variables for a stochastically moving optimum.

Table S4 The variability in aspects of the **G**-matrix and stability of these variables, as measured by the within-run standard deviations.

Table S5 Combinations of simulation parameters that resulted in the population dropping below the carrying capacity (indicated by XX in the table below), a condition that meant the population could no longer replace itself and was on the road to extinction.

Figure S1 The relationship between lag and eccentricity, as well as eccentricity and the per-generation change in the angle of **G**, under an episodically moving optimum.

As a service to our authors and readers, this journal provides supporting information supplied by the authors. Such materials are peer-reviewed and may be re-organized for online delivery, but are not copy-edited or typeset. Technical support issues arising from supporting information (other than missing files) should be addressed to the authors.

Received 7 October 2011; revised 15 June 2012; accepted 9 July 2012